The Astrophysical Journal, 703:1203–1223, 2009 October 1 doi:10.1088/0004-637X/703/2/1203

DIAGNOSTIC LINE EMISSION FROM EXTREME ULTRAVIOLET AND X-RAY-ILLUMINATED DISKS AND SHOCKS AROUND LOW-MASS STARS

David Hollenbach[1] and U. Gorti[1,2]
[1] SETI Institute, 515 North Whisman Road, Mountain View, CA 94043, USA
[2] NASA Ames Research Center, Moffett Field, CA 94035, USA
Received 2009 June 4; accepted 2009 August 6; published 2009 September 8

ABSTRACT

Extreme ultraviolet (EUV; 13.6 eV $< h\nu \lesssim$ 100 eV) and X-rays in the 0.1–2 keV band can heat the surfaces of disks around young, low-mass stars to thousands of degrees and ionize species with ionization potentials greater than 13.6 eV. Shocks generated by protostellar winds can also heat and ionize the same species close to the star/disk system. These processes produce diagnostic lines (e.g., [Ne II] 12.8 μm and [O I] 6300 Å) that we model as functions of key parameters such as EUV luminosity and spectral shape, X-ray luminosity and spectral shape, and wind mass loss rate and shock speed. Comparing our models with observations, we conclude that either internal shocks in the winds or X-rays incident on the disk surfaces often produce the observed [Ne II] line, although there are cases where EUV may dominate. Shocks created by the oblique interaction of winds with disks are unlikely [Ne II] sources because these shocks are too weak to ionize Ne. Even if [Ne II] is mainly produced by X-rays or internal wind shocks, the neon observations typically place upper limits of $\lesssim 10^{42}$ s^{-1} on the EUV photon luminosity of these young low-mass stars. The observed [O I] 6300 Å line has both a low velocity component (LVC) and a high velocity component. The latter likely arises in internal wind shocks. For the former we find that X-rays likely produce more [O I] luminosity than either the EUV layer, the transition layer between the EUV and X-ray layer, or the shear layer where the protostellar wind shocks and entrains disk material in a radial flow across the surface of the disk. Our soft X-ray models produce [O I] LVCs with luminosities up to $10^{-4}\ L_\odot$, but may not be able to explain the most luminous LVCs.

Key words: circumstellar matter – infrared: stars – planetary systems: protoplanetary disks – stars: formation – stars: winds, outflows – X-rays: stars

1. INTRODUCTION

The photoevaporation of a protoplanetary disk by the extreme ultraviolet (EUV; 13.6 eV $< h\nu \lesssim$ 100 eV) or Lyman continuum photons from the central star may significantly affect the formation and evolution of planets and planetesimals, and may be one of the important mechanisms for dispersing disks (Hollenbach et al. 1994, 2000; Clarke et al. 2001; Richling et al. 2006; Alexander et al. 2006a, 2006b; Alexander 2008a). EUV photoevaporation occurs because the EUV photons create a 10^4 K, ionized surface on the disk, and beyond about $1(M_*/1\ M_\odot)$ AU, where M_* is the stellar mass, the thermal pressure of the gas is sufficient to drive a significant hydrodynamic flow out of the gravitational potential of the star and into interstellar space.

Some of the most detailed models of the dispersal of disks around isolated low-mass stars invoke viscous spreading and accretion on the inside ($\lesssim$ few AU) of the disk and EUV-induced photoevaporation on the outside (Clarke et al. 2001; Matsuyama et al. 2003; Ruden 2004; Alexander et al. 2006a, 2006b). This combination has been invoked to explain gas-poor giants such as Uranus and Neptune (Shu et al. 1993), the rapid evolution of classical T Tauri stars to weak-lined T Tauri stars (Clarke et al. 2001; Alexander et al. 2006a, 2006b), the production of large inner holes such as exist in some sources (Alexander 2008a; Cieza et al. 2008), and the migration and "parking" of giant planets (Matsuyama et al. 2003; Lecar & Sasselov 2003; Veras & Armitage 2004).

X-rays from the star also significantly affect the disk. Glassgold et al. (2004) show that hard X-rays can penetrate to moderate depths into the disk and produce sufficient ionization to maintain a vigorous magnetorotational instability (MRI; Balbus & Hawley 1991), at least in the upper layers of the disk (see also Sano et al. 2000; Stone & Pringle 2001). Chiang & Murray-Clay (2007) have recently expanded on this idea, using X-rays to stimulate MRI in the inner edge of a dusty disk, thereby eating away the disk from inside out. Alexander et al. (2004a) have argued that X-rays by themselves do not lead to significant photoevaporation, but Gorti & Hollenbach (2009) have shown that ~1 keV X-rays may increase far ultraviolet (FUV)-induced photoevaporation rates by roughly a factor of 2, because X-ray ionization increases the electron abundance, which enhances the FUV grain photoelectric heating mechanism. More recently (Ercolano et al. 2008, 2009; Gorti et al. 2009), it has become clear that a soft (0.1–0.5 keV) X-ray component can lead to significant photoevaporation rates. Glassgold et al. (2007) and Meijerink et al. (2008) have shown that X-rays partially ionize and heat the gas just below the EUV fully ionized layer and that the X-ray-heated gas achieves temperatures of order 1000–4000 K in a dense ($n \sim 10^7$ cm^{-3}) layer out to about 10–20 AU. Although they do not discuss X-ray photoevaporation, these temperatures, densities, and radii suggest significant rates.

EUV and X-ray photons around low-mass stars, whose photospheres are too cool to produce a substantial EUV or X-ray flux, emanate from the accretion shock created by the impact of the accreting disk gas onto the stellar surface and/or from the hot plasma generated by magnetic activity on the stellar surface akin to (but much greater than) the Sun's chromosphere or corona. These two mechanisms heat plasma to temperatures $\gg 10^4$ K, and thereby produce significant EUV and X-ray luminosity. Alexander et al. (2004b) argue that the EUV photons do not likely penetrate the accretion columns to irradiate the disk and that, therefore, magnetic activity is

a more attractive source for the EUV that shines on the disk surface. However, many accreting sources exhibit a soft X-ray component (e.g., Kastner et al. 2002; Stelzer & Schmitt 2004), which may arise from an accretion shock or is at least mediated by accretion flows (Preibisch 2007; Güdel & Telleschi 2007). Soft X-rays are only somewhat more penetrating than EUV photons, raising the possibility that the geometry of the accretion streams (sometimes called "funnel flows") onto the star may also allow the escape of at least some of these hydrogen-ionizing photons. The hard ($\gtrsim$1 keV) X-rays likely arise from the magnetic activity (i.e., the chromosphere and corona).

Whatever the source of EUV photons, they must still penetrate protostellar winds. Protostellar winds are thought to be driven by magnetohydrodynamic processes from the inner portions of accreting disks (e.g., Shu et al. 1994; Ouyed & Pudritz 1997). We show in Section 2 that these winds must have low-mass loss rates, $\dot{M}_{\rm w} \lesssim 10^{-9}\,M_\odot$ yr^{-1}, for EUV or soft ($\lesssim$0.2 keV) X-rays to penetrate them and to illuminate the disk surface beyond $\sim$1 AU, where photoevaporation proceeds. Since accretion rates onto the central star are correlated with protostellar wind mass loss rates (Hartigan et al. 1995; White & Hillenbrand 2004), this critical wind mass loss rate corresponds to an accretion rate of about $10^{-8}\,M_\odot$ yr^{-1}.

The main weakness in EUV photoevaporation models is the extreme uncertainty in the EUV photon luminosity $\Phi_{\rm EUV}$ of the central star. The EUV opacity of hydrogen is so high that a column of only $\sim 10^{17}$ hydrogen atoms cm^{-2} provides optical depth of order unity. Therefore, interstellar extinction prevents the direct observation of the EUV flux from young, low-mass stars with disks. There are, however, observations of nearby, older, solar-mass stars, including the Sun, which provide a clue to the spectra from the FUV (6 eV $< h\nu <$ 13.6 eV) to the X-ray of low-mass stars due to their magnetic activity (Ribas et al. 2005). These suggest that, very roughly, νF_ν is constant for a given star from the FUV band through the EUV band to the keV X-ray band. Ercolano et al. (2009) also discussed observations of flare stars that suggest magnetically heated coronae on the stellar surfaces with a range of plasma temperatures resulting in roughly an $F_\nu \propto \nu^{-1}$ power-law EUV spectrum. Thus, one might estimate the magnetically produced EUV luminosity of a low-mass star by measuring either (or both) the 0.1–1.0 keV X ray luminosity or the 6–13.6 eV FUV luminosity. For nonaccreting but young ($\sim$1 Myr) low-mass stars, the X-ray and FUV luminosities tend to be of order $\sim 10^{-3}$ $L_{\rm bol}$ (e.g., Flaccomio et al. 2003; Valenti et al. 2003), suggesting $L_{\rm EUV} \sim 10^{-3} L_\odot$ or $\Phi_{\rm EUV} \sim 10^{41}$ EUV photons per second for a 1 $M_\odot$ star.

Alexander et al. (2005), based on earlier work of Brooks et al. (2001), used FUV emission lines of various ions of the elements carbon, oxygen, nitrogen, and silicon seen in T Tauri stars to try to estimate the distribution of emission measures as a function of T of the hot ($\sim 10^4$–10^6 K) plasma. As the authors themselves point out, this method is fraught with difficulties, and, as a result, they can only constrain $\Phi_{\rm EUV}$ to range from 10^{41} to 10^{44} s^{-1} in young solar mass stars. The knowledge of the EUV luminosity is critical in predicting EUV-driven photoevaporation and determining whether it dominates disk evolution and explains the observed short ($\sim$1–3 Myr) lifetimes of disks around low-mass stars.

One way to measure $\Phi_{\rm EUV}$ is to observe emission lines produced by the heating and ionization caused by these photons on the disk surface. Such a measurement is important since $\Phi_{\rm EUV}$ determines the EUV photoevaporation rates and therefore the EUV-induced dispersal times of the gas and dust in these young, planet-forming disks. Given a disk illuminated by EUV photons, a tenuous, 10^4 K, fully ionized surface is created by the photoionization of hydrogen. In effect, a sort of "blister H II region" is created above the bulk of the disk, which is mostly neutral molecular gas. Although this H II region contains very little mass ($\sim 10^{-7}[\Phi_{\rm EUV}/10^{41}\ {\rm s}^{-1}]^{1/2} M_{\rm J}$, where $M_{\rm J}$ is the Jupiter mass), it can produce sufficient forbidden optical line emission (e.g., [S II] 6731 Å and [N II] 6583 Å; see Font et al. 2004) or infrared (IR) fine structure emission (e.g., [Ne II] 12.8 μm; this paper) to be observed. We note that [Ne II] 12.8 μm is one of the strongest lines from H II regions associated with Giant Molecular Clouds, and, because neon is not depleted and its gas phase abundance relative to hydrogen is quite well known, this fine structure line can also be used in these regions to measure or constrain the ionizing luminosity of the exciting star(s) (Ho & Keto 2007).

There are two problems in using the emission lines from the H II surface to measure $\Phi_{\rm EUV}$. Uncertainties in extinction, the gas temperature, and the gas density make the *optical* lines a poor diagnostic of $\Phi_{\rm EUV}$. The IR fine structure lines are much better for this purpose, but they can also be produced by the heating and (partial) ionization of the neutral gas below the H II surface by penetrating X-rays (Glassgold et al. 2007). In addition, they can be produced in high velocity (ionizing) shocks created by the protostellar wind. We discuss in this paper the relative contributions to the fine structure emission by the surface EUV-heated layer, the subsurface X-ray-heated layer, and the wind shocks. However, even if its origin cannot be distinguished, the fine structure emission, for example, [Ne II] 12.8 μm, gives a strict upper limit on $\Phi_{\rm EUV}$. In addition, if arising from the EUV or X-ray layers, the [Ne II] and other fine structure lines provide a measure of the density and temperature of the hot surface gas and therefore directly probe some of the regions where photoevaporation originates (Alexander 2008b).

[Ne II] 12.8 μm emission from young stars with optically thick disks was first detected using the high resolution mode of the infrared spectrograph (IRS) instrument on the *Spitzer Space Telescope* (Pascucci et al. 2007; Lahuis et al. 2007; Ratzka et al. 2007; Espaillat et al. 2007), and is now found in over $\sim$50 sources (Güdel et al. 2009). Some of these sources ($\sim$15) also show emission from the hydrogen recombination lines H(7–6)α and H(6–5)α, and only one source is detected in [Ne III]15 μm. Observed line luminosities range from 10^{-4} to 10^{-6} $L_\odot$. Follow-up, very high resolution ground-based observations of some bright [Ne II] sources have resolved the line emission and observed line widths ($\sim$15–80 km s^{-1}), interpreted as emission arising from X-ray-heated layers in Keplerian-rotating disks (Herczeg et al. 2007; Najita et al. 2009), EUV photoevaporative flows (Herczeg et al. 2007; Pascucci & Sterzik 2009), or outflows associated with these sources (van Boekel et al. 2009; Najita et al. 2009). Correlations have been sought between the [Ne II] luminosities and disk and stellar diagnostics such as X-ray luminosity (Pascucci et al. 2007; Güdel et al. 2009) and mass accretion rates (Espaillat et al. 2007; Güdel et al. 2009), but the data are inconclusive. The origin of the [Ne II] emission, although widely attributed to disks, is still not definitive.

This paper is motivated by the recent observations of [Ne II] 12.8 μm emission. We model disks illuminated by EUV and X rays, and present results for the IR fine structure lines of Ar^+, Ar^{++}, Ne^+, Ne^{++}, N^+, N^{++}, O^{++}, S^{++}, and S^{+++}, two IR recombination lines of H, and the optical forbidden line [O I] 6300 Å. We

show that if the EUV layer dominates the emission, the IR fine structure lines diagnose $\Phi_{\rm EUV}$ and the shape (slope) of the EUV spectrum. We also show that measurements of [Ne II] 12.8 μm and [Ne III] 15 μm are particularly good diagnostics of these parameters, being strong and relatively insensitive to extinction and changes in the plasma density n or temperature T. Our models of the X-ray layers, like the X-ray models of Glassgold et al. (2007) and Meijerink et al. (2008), produce [Ne II] emission that, at least in some cases, is in accord with the observations. However, in a number of cases the X-ray heating mechanism seems insufficient to provide the emission (Espaillat et al. 2007; Güdel et al. 2009), as we will also show in this paper. Shocks in the protostellar wind or an unseen EUV or soft (∼0.1–0.3 keV) X-ray component may provide the origin of [Ne II] in these cases. Our models differ from Glassgold et al. in that we treat the vertical structure of the disk consistently (i.e., the gas temperature is not assumed to equal the dust temperature in calculating the vertical density structure), include EUV ionization and heating, include FUV photodissociation and heating, treat the X-ray heating somewhat differently, and include some additional significant cooling lines, such as [Ne II] 12.8 μm and [Ar II] 7 μm.

This paper complements earlier (Gorti & Hollenbach 2004, 2008) papers, which examined the molecular and atomic fine structure emission from the neutral disk. In this older work, the fine structure lines treated focused mainly on those with ionization potentials (IPs) less than 13.6 eV, such as those of O, C, C^+, S, Si, Si^+, Fe, and Fe^+, although we did treat the X-ray ionization of some species in the predominantly neutral gas. In this paper we focus on species with IPs greater than 13.6 eV, which are only found in the fully photoionized H II region surfaces of disks, in X-ray-ionized, predominantly neutral gas, or in fast ($\gtrsim$100 km s^{-1}) shocks produced by the stellar wind.

We organize the paper as follows. We discuss the restriction on the wind mass loss rate in order for the FUV, EUV, and X-ray radiation from the protostar to penetrate the wind and shine on the disk surface in Section 2. Section 3 provides analytic estimates of the relation of the fine structure and hydrogen recombination line luminosities to $\Phi_{\rm EUV}$, the scaling of the emission from the X-ray layer to the X-ray luminosity of the central star, the [Ne II] luminosity produced in wind shocks, and the [O I] 6300 Å luminosity possible from both the disk and wind shocks. Section 4 shows the results of numerical models. Section 5 compares the results of our models to recent observations made by the *Spitzer Space Telescope* and several ground-based telescopes, and discusses the relative contributions of EUV, X rays, and shocks to the observed [Ne II], hydrogen recombination lines, and [O I] emission. We conclude with a discussion and summary in Section 6.

2. FAR-ULTRAVIOLET, EXTREME ULTRAVIOLET, AND X-RAY PENETRATION OF PROTOSTELLAR WINDS

Although our protostellar wind model is influenced by the "X wind" models of Shu et al. (1994), the main assumption we make is that the bulk of the wind mass loss rate $\dot{M}_{\rm w}$ originates from cylindrical radius $r_{\rm w}$ to $r_{\rm w} + f r_{\rm w}$, where $r_{\rm w} \sim 10^{12}$ cm and $f \sim 1$. Therefore, the model also applies to other disk wind models (e.g., Ouyed & Pudritz 1997) where the bulk of the mass loss originates from the inner disk surface. We assume that f is sufficiently small that we can take n_b as the average hydrogen nucleus density at the base of the wind without introducing significant error by assuming this constant density from $r_{\rm w}$ to $r_{\rm w} + f r_{\rm w}$.

The mass loss in the wind, $\dot{M}_{\rm w}$, arising from this geometry is given as

$$\dot{M}_{\rm w} = 2\left[\pi (r_{\rm w} + f r_{\rm w})^2 - \pi r_{\rm w}^2\right] n_b m_{\rm H} v_{\rm w}, \quad (1)$$

where $m_{\rm H} = 2.3 \times 10^{-24}$ g is the mass per hydrogen nucleus and $v_{\rm w}$ is the wind velocity. The hydrogen nucleus column density $N_{\rm w}$ through the base of the wind, which the energetic photons must penetrate to reach the outer disk surface, is then given as

$$N_{\rm w} \simeq n_b f r_{\rm w} \simeq 2.2 \times 10^{21} \left(\frac{\dot{M}_{\rm w}}{10^{-8}\ M_\odot\ {\rm yr}^{-1}}\right) \left(\frac{100\ {\rm km\ s}^{-1}}{v_{\rm w}}\right) \times \left(\frac{10^{12}\ {\rm cm}}{r_{\rm w}}\right) \left(\frac{1}{1+0.5f}\right)\ {\rm cm}^{-2}. \quad (2)$$

Interstellar dust requires a hydrogen nucleus column of $\sim 10^{21}$ cm^{-2} to provide optical depth unity in the FUV. However, the dust lifted from the surface of the disk at the base of the wind is likely to have coagulated to much larger sizes than interstellar dust and furthermore to have lower dust/gas mass ratios because of sublimation of the less refractory materials and settling of the refractory grains to the midplane (Dullemond & Dominik 2005). In fact, at radii of $\lesssim 10^{12}$ cm it is possible that all dust has sublimated. All these processes lower the dust cross section per hydrogen nucleus. Even if there is no dust (e.g., if all the dust is sublimated), the gas provides FUV opacity and attenuates the FUV significantly for columns greater than about 10^{24} cm^{-2}. Assuming a minimum reduction in dust opacity relative to interstellar dust of a factor of 10, FUV will penetrate wind columns $N_{\rm w} \lesssim 10^{22}$ cm^{-2}. Dust also provides a source of X-ray opacity, which will be reduced from interstellar values by the effects of settling and coagulation. However, considerable opacity remains in the gas phase elements such as C, O, and Ne. Gorti & Hollenbach (2004, 2008) estimated, using the cross sections of Wilms et al. (2000), that $N_{\rm w} \sim 10^{22}$ cm^{-2} is required for 1 keV optical depth unity at disk surfaces. On the other hand, soft X-rays experience considerably more optical depth, and $N_{\rm w} \sim 10^{20}$ cm^{-2} provides optical depth unity for ∼0.2 keV X-rays. Therefore, in summary, $\dot{M}_{\rm w} \lesssim 4 \times 10^{-8}\ M_\odot$ yr^{-1} is required for ∼1 keV X-rays to penetrate the protostellar wind, whereas soft X-rays can only penetrate when $\dot{M}_{\rm w} \lesssim 4 \times 10^{-10}\ M_\odot$ yr^{-1}. The penetration of the FUV likely occurs at mass loss rates considerably higher than $\dot{M}_{\rm w} \sim 4 \times 10^{-8}\ M_\odot$ yr^{-1} because of dust sublimation and settling, but this number serves as a useful lower limit.

A column $N_{\rm w}$ of 10^{20}–10^{22} cm^{-2} of *neutral* hydrogen is totally opaque to EUV photons, since $N({\rm H\,I}) \sim 10^{17}$–$10^{18}$ cm^{-2} produces EUV optical depth unity. For EUV photons to penetrate the wind, the EUV photon flux $F_{\rm EUV}$ must be sufficiently high to keep the base of the wind fully ionized, so that $n({\rm H\,I})/n_b \ll 1$ and $N({\rm H\,I}) \lesssim 10^{17}$ cm^{-2}. This "Strömgren" condition

$$F_{\rm EUV} > \alpha_{r,H} n_b^2 f r_{\rm w} \quad (3)$$

can be rewritten as

$$\dot{M}_{\rm w} \lesssim 8 \times 10^{-10} \left(\frac{f r_{\rm w}}{10^{12}\ {\rm cm}}\right)^{1/2} \left(\frac{\Phi_{\rm EUV}}{10^{41}\ {\rm s}^{-1}}\right)^{1/2} \times \left(\frac{v_{\rm w}}{100\ {\rm km\ s}^{-1}}\right)\ M_\odot\ {\rm yr}^{-1}. \quad (4)$$

In other words, the mass loss rate has to be less than the right-hand side of this equation for EUV to penetrate the base of the wind and illuminate the outer disk surface beyond 1 AU.

Wind mass loss rates are hard to measure "directly" from the observed optical line emission (e.g., [S II]) seen in their jets. The derived mass loss rates from these optical lines depend on knowing the gas temperature, the gas density, and the ionized fraction—all of which are quite uncertain. "Indirect" methods rely on measuring the momentum in swept-up circumstellar gas. This method is also approximate since it requires an estimate of the wind speed, the duration of the mass loss episode, and the conversion factor of CO luminosity to mass. Likewise there are uncertainties in observationally determining the mass accretion rate $\dot{M}_{\rm acc}$ onto the central star. These uncertainties create a spread in the constant k of proportionality, but it is generally agreed that the wind mass loss rate scales with the mass accretion rate, $\dot{M}_{\rm w} \simeq k\dot{M}_{\rm acc}$. The constant k has been estimated from ∼0.01 (Hartigan et al. 1995) to ∼0.1 (White & Hillenbrand 2004). The Shu et al. (1994) X wind model predicts values somewhat higher than 0.1. White and Hillenbrand pointed out that there seems to be considerable *intrinsic* scatter in the ratio of wind mass loss rate to mass accretion rate from source to source.

Roughly then, if we take $\dot{M}_{\rm w} \sim 0.1\dot{M}_{\rm acc}$, the FUV and ∼1 keV X-rays penetrate the wind when $\dot{M}_{\rm acc} \lesssim 4 \times 10^{-7}\, M_\odot$ yr^{-1}, whereas the EUV and soft (∼0.2 keV) X-rays penetrate the wind when the accretion rate has dropped to $\dot{M}_{\rm acc} \lesssim 8 \times 10^{-9}\, M_\odot$ yr^{-1}. Hartmann et al. (1998) show the evolution of $\dot{M}_{\rm acc}$ for young, solar mass stars. With order of magnitude dispersion, $\dot{M}_{\rm acc}$ is roughly $10^{-8}\, M_\odot$ yr^{-1} at 1 Myr, and drops rapidly on Myr timescales. Thus, FUV and ∼ 1 keV X rays illuminate the disk surface nearly as soon as the epoch of heavy accretion of material onto disk and star from the natal cloud core has ceased. However, EUV and soft X-rays may not illuminate the disk surface until roughly 1–2 Myr has elapsed from that time.

If one wishes to observe a disk whose ionized fine structure lines are not produced by EUV and soft X-rays, one should select sources with $\dot{M}_{\rm acc} \gtrsim 8 \times 10^{-9} M_\odot$ yr^{-1}. If [Ne II], for example, is detected in sources with $8 \times 10^{-9} M_\odot$ yr$^{-1} \lesssim \dot{M}_{\rm acc} \lesssim 4 \times 10^{-7}\, M_\odot$ yr^{-1}, then hard (∼1 keV) X-rays or possibly wind shocks may be implicated. If [Ne II] is detected in sources with $\dot{M}_{\rm acc} \gtrsim 4 \times 10^{-7}\, M_\odot$ yr^{-1}, then protostellar wind shocks almost certainly provide the origin. If one wishes to observe sources illuminated by both X-rays and EUV, and therefore containing, for example, [Ne II] emission from an EUV-produced H II surface and also from an X-ray-produced partially ionized deeper layer, then one should observe sources with $\dot{M}_{\rm acc} \lesssim 8 \times 10^{-9}\, M_\odot$ yr^{-1}. Interestingly, the [Ne II] sources have been detected in [Ne II] emission in this entire range of $\dot{M}_{\rm acc}$, suggesting a wide range of origin of [Ne II] (see Espaillat et al. 2007; Güdel et al. 2009).

3. ANALYTIC MODELS OF EMISSION LINES DIAGNOSTIC OF EUV AND X-RAYS INCIDENT ON DISKS OR OF SHOCKS

There are basically three types of lines diagnostic of EUV and X-rays incident on disks or of fast, ionizing shocks in protostellar winds: hydrogen recombination lines, optical forbidden lines such as [O I] 6300 Å, [S II] 6713 and 6731 Å, and [N II] 6583 Å, and the IR fine structure lines of ionized species whose ionization requires photons more energetic than 13.6 eV. We discuss here the last two and leave the discussion of hydrogen recombination lines for Section 3.2. With the possible exception of [O I] 6300 Å, the optical lines likely arise in the completely ionized H II region at the surface of the disk or in fast, ionizing shocks because the lines typically lie ≳20,000 K above ground and are excited mainly by electron collisions; these regions have higher temperatures (∼10^4 K versus several thousand K in the X-ray-heated region) and generally higher electron densities than the X-ray layers. In addition, most of the optical lines arise from ionized species whose abundances peak in the completely ionized H II gas as opposed to the mostly neutral X-ray layers (the notable exception being [O I]). The IR fine structure lines from high IP (>13.6 eV) species typically lie ∼300–1000 K above ground and therefore are not sensitive to temperature for temperatures above about 300–1000 K. These lines may come from either the EUV-heated H II region, the X-ray-heated region, or shocked regions and we show below that the relative EUV versus X-ray photon luminosity from the central star determines which of these two regions will dominate the emission. We focus in this section on the IR lines, because Font et al. (2004) and Meijerink et al. (2008) have discussed the optical emission from the EUV and X-ray-heated layers. However, we do include the [O I] 6300 Å line in our analysis, because our [O I] luminosities from the X-ray layer differ from the Meijerink et al. values, and because other researchers have not been able to match the observed luminosities in this line (Hartigan et al. 1995). We also include a discussion of the IR hydrogen recombination lines that have been observed from these star/disk systems.

3.1. Fine Structure Lines from the H II Surface (EUV Layer)

Consider an axisymmetric disk described by cylindrical coordinates r, z. If $f_{\rm EUV}$ is the fraction of ionized photons from the star absorbed by the disk, then the Strömgren condition is

$$f_{\rm EUV}\Phi_{\rm EUV} = 2\alpha_{r,H}\int_{z_{IF}}^{\infty} dz \int_{r_i}^{r_o} 2\pi r n_{\rm e}^2 dr, \qquad (5)$$

where the electron density $n_{\rm e}$ is a function of r and z but is negligible below $z_{\rm IF}$, the ionization front, and where we have ignored dust attenuation in the H II surface region above $z_{\rm IF}$. We will justify the neglect of dust post facto below, as well as show that $f_{\rm EUV} \sim 0.7$. In Equation (5) $r_{\rm i}$ and $r_{\rm o}$ are the inner and outer radii of the disk, and $\alpha_{r,H}$ is the case B recombination coefficient for electrons with protons ($\alpha_{r,H} = 2.53 \times 10^{-13}$ cm^3 s^{-1} at $T = 10^4$ K; Storey & Hummer 1995).

For simplicity, we treat the specific example of a simple two-level fine structure system such as [Ne II] 12.8 μm. Then, for a transition t the escaping line luminosity L_t from the disk is given as

$$L_t \simeq \gamma_t \Delta E_t \int_{z_{IF}}^{\infty} dz \int_{r_{\rm i}}^{r_{\rm o}} 2\pi r \left(\frac{n_{\rm e} n(i)}{1 + \frac{n_{\rm e}}{n_{{\rm ecr},t}}}\right) dr, \qquad (6)$$

where γ_t is the collisional excitation rate coefficient of the transition, ΔE_t is the photon energy, $n_{{\rm ecr},t}$ is the critical electron density for the transition, and $n(i)$ is the density of the ionized species i that produces the transition. Note that here we have included the fact that half the emitted IR photons are directed toward the disk midplane, where they are absorbed by the (assumed) optically thick disk and half escape. If we set $n(i) = x_s f(i) n_{\rm e}$, where x_s is the abundance of species s (in all ionization states) in the EUV layer, and $f(i)$ is the fraction of that species in ionization state i, then we can write using Equation (5)

$$L_t = \gamma_t \Delta E_t \left(\frac{f_{\rm EUV}\Phi_{\rm EUV} x_s f(i)}{2\alpha_{r,H}}\right)\left(\frac{1}{1 + \frac{n_{\rm e}}{n_{{\rm ecr},t}}}\right). \qquad (7)$$

Table 1
IR Fine Structure Parameters for Species in Ionized Gas

Transition	C_t (erg)	$n_{\mathrm{ecr},s}$ (cm^{-3})	$x(s)$	Refs.
[Ar II] 7 μm	1.8(−13)	4.2(5)	6.3(−6)[a]	1
[Ar III] 9 μm	3.7(−14)	1.2(6)	6.3(−6)[a]	2
[N II] 122 μm	2.3(−14)	1.6(3)	9.1(−5)[a]	3
[N III] 58 μm	5.0(−13)	1.2(3)	9.1(−5)[a]	4
[Ne II] 12.8 μm	2.2(−13)	6.3(5)	1.2(−4)[b]	5
[Ne III] 15.0 μm	3.7(−13)	2.7(5)	1.2(−4)[b]	6
[O III] 52 μm	8.3(−13)	4.6(3)	3.2(−4)[a]	3
[S III] 18 μm	3.3(−13)	1.5(4)	7.6(−6)[c]	7
[S III] 33 μm	3.0(−13)	4.1(3)	7.6(−6)[c]	7
[S IV] 10.4 μm	9.5(−14)	4.0(5)	7.6(−6)[c]	8

Notes.
Abundances are from:
[a] Savage & Sembach (1996).
[b] Grevesse & Sauval (1998).
[c] Asplund et al. (2005).
References. (1) Pelan & Berrington 1995; (2) Galavis et al. 1995; (3) Lennon & Burke 1994; (4) Blum & Pradhan 1992; (5) Griffin et al. 2001; (6) Butler & Zeippen 1994; (7) Tayal & Gupta 1999; (8) Tayal 2000.

We note that in taking $x_s f(i)$ out of the integral in Equation (6) we implicitly assume that in Equation (7) $x_s f(i)$ is the density-weighted average of this product in the EUV layer. Thus, we find that if $n_{\mathrm{e}} < n_{\mathrm{ecr},t}$ and if $f(i)$ does not depend on Φ_{EUV} (e.g., for the dominant ionization state where $f(i) \simeq 1$), then the line luminosity L_t is directly proportional to the ionizing photon luminosity Φ_{EUV} of the central star. If EUV is the sole excitation source, the measurement of L_t directly measures the uncertain parameter Φ_{EUV} if we have knowledge of x_s and $f(i)$. The main unknown is the fraction $f(i)$ in a particular ionization state i, since the gas phase abundance of an element can often be estimated from observations of H II regions. For example, neon is often found as Ne^{+} and Ne^{++}. We therefore rewrite Equation (7) as

$$L_t = C_t f(i) f_{\mathrm{EUV}} \Phi_{\mathrm{EUV}} \left(\frac{1}{1 + \frac{n_{\mathrm{e}}}{n_{\mathrm{ecr},t}}} \right), \tag{8}$$

where $C_t \equiv \gamma_t \Delta E_t x_s / (2\alpha_{r,H})$. Note that C_t and $n_{\mathrm{ecr},t}$ are known quantities and therefore constants in the equation. If the transition is from the dominant ionization state of the species, then $f(i) \sim 1$. Our modeling of disks suggests $f_{\mathrm{EUV}} \sim 0.7$. C_t is therefore the main constant of proportionality that links the observed IR line luminosity to the EUV photon luminosity; for $n_{\mathrm{e}} < n_{\mathrm{ecr},t}$ and taking the dominant ionization state, C_t is the energy per absorbed EUV photon that emerges from the disk in the fine structure transition. Table 1 lists the value of C_t for the various transitions considered in this paper, along with $n_{\mathrm{ecr},t}$ and the assumed x_s that is used in C_t.

The above equations show that it is important to estimate the electron density in the ionized surface of the disk at the radius where most of the emission in a given line is produced. We follow the results of Hollenbach et al. (1994). Because the H II region surface is isothermal, the electron density at a given r decreases from z_{IF} upward as

$$n_{\mathrm{e}}(r, z) = n_{\mathrm{e}}(r, z_{\mathrm{IF}}) e^{-\left(\frac{z - z_{\mathrm{IF}}}{2H}\right)^2}, \tag{9}$$

where H is the isothermal scale height of the 10^4 K gas given by

$$H(r) = r_{\mathrm{g}} \left(\frac{r}{r_{\mathrm{g}}} \right)^{3/2} \tag{10}$$

for $r < r_{\mathrm{g}}$, and where r_{g} is given by

$$r_{\mathrm{g}} \simeq 7 \left(\frac{M_*}{1\ M_\odot} \right) \mathrm{AU}. \tag{11}$$

Note that in Equation (9), both z_{IF} and H are functions of r. The gravitational radius r_{g} is where the sound or hydrogen thermal speed is equal to the escape speed from the gravitational potential of the star. For $r > r_{\mathrm{g}}$, where the gas is freely evaporating, the effective height of the disk is $H \sim r$, since the initially vertically flowing gas turns over on radial streamlines by the time $z = r$. Hollenbach et al. also showed that the base electron density at z_{IF} falls off radially as a power law:

$$n_{\mathrm{e}}(r, z_{\mathrm{IF}}) \simeq 5 \times 10^4 \left(\frac{\Phi_{\mathrm{EUV}}}{10^{41}\ \mathrm{s}^{-1}} \right)^{1/2} \left(\frac{r_{\mathrm{g}}}{r} \right)^{3/2} \times \left(\frac{1\ M_\odot}{M_*} \right)^{3/2} \mathrm{cm}^{-3} \quad \text{for } r < r_{\mathrm{g}} \tag{12}$$

and

$$n_{\mathrm{e}}(r, z_{\mathrm{IF}}) \simeq n_{\mathrm{e}}(r_{\mathrm{g}}, z_{\mathrm{IF}}) \left(\frac{r_{\mathrm{g}}}{r} \right)^{5/2} \quad \text{for } r > r_{\mathrm{g}}. \tag{13}$$

Note that if $n_{\mathrm{e}}(r, z_{\mathrm{IF}}) < n_{\mathrm{ecr}}$ everywhere, then the amount of luminosity $L(r)$ from a logarithmic interval of r is proportional to the volume emission measure $n_{\mathrm{e}}^2 V$ at that r, or to $n_{\mathrm{e}}^2 r^2 H$. For $r < r_{\mathrm{g}}$ we then obtain $L(r) \propto r^{1/2}$ whereas for $r > r_{\mathrm{g}}$ we obtain $L(r) \propto r^{-2}$. In other words, the line luminosity originates mostly from $r \sim r_{\mathrm{g}}$. If the electron densities in the very inner regions exceed n_{ecr} but are less than n_{ecr} at r_{g}, the luminosity is relatively unaffected, and our conclusion does not change. However, if $n_{\mathrm{e}}(r_{\mathrm{g}}, z_{\mathrm{IF}}) > n_{\mathrm{ecr}}$, then the line luminosity will drop. The line emissivity will be suppressed by a factor of approximately $n_{\mathrm{e}}(r_{\mathrm{g}}, z_{\mathrm{IF}})/n_{\mathrm{ecr}}$ at r_{g}. However, now $L(r) \propto n_{\mathrm{e}} V$ as long as $n_{\mathrm{e}} > n_{\mathrm{ecr}}$, so that $L(r) \propto r^{1/2}$ beyond r_{g} until the density drops below the critical density, when it reverts to its former r^{-2} dependence. The luminosity of a low critical density species will therefore originate from the radius

$$r_{\mathrm{max}} = \left(\frac{n_{\mathrm{e}}(r_{\mathrm{g}}, z_{\mathrm{IF}})}{n_{\mathrm{ecr}}} \right)^{2/5} r_{\mathrm{g}}, \tag{14}$$

where $n_{\mathrm{e}}(r_{\mathrm{max}}, z_{\mathrm{IF}}) = n_{\mathrm{ecr}}$. As a result,

$$L \propto n_{\mathrm{e}}(r_{\mathrm{max}}, z_{\mathrm{IF}}) r_{\mathrm{max}}^3 \propto \Phi_{\mathrm{EUV}}^{3/5} \tag{15}$$

as long as $n_{\mathrm{e}}(r_{\mathrm{g}}, z_{\mathrm{IF}}) > n_{\mathrm{ecr}}$ and $f(i)$ is constant.

As examples, consider [Ne II] 12.8 μm and [S III] 19 μm. The critical density for [Ne II] is given as $n_{\mathrm{ecr,[Ne\,II]}} \equiv A_{21}/\gamma_{21} \simeq 6 \times 10^5\ \mathrm{cm}^{-3}$, where we have taken $A_{21} = 0.00859\ \mathrm{s}^{-1}$ and a collisional de-excitation rate coefficient at 10^4 K of $\gamma_{21} = 1.355 \times 10^{-8}\ \mathrm{cm}^3\ \mathrm{s}^{-1}$ (Griffin et al. 2001). Thus, comparing this critical density with the electron density at r_{g} (Equation (12)), we see that [Ne II] is subthermal at r_{g} typically and that therefore it mostly originates from r_{g} and tracks Φ_{EUV} linearly as long as $f(\mathrm{Ne}^{+})$ is constant. However, [S III] has a critical density of approximately $5 \times 10^3\ \mathrm{cm}^{-3}$ which is about 10 times less than $n_{\mathrm{e}}(r_{\mathrm{g}}, z_{\mathrm{IF}})$ for a solar mass star with $\Phi_{\mathrm{EUV}} \sim 10^{41}\ \mathrm{s}^{-1}$ (see Equation (12)). Therefore, $r_{\mathrm{max}} \simeq 10^{2/5} r_{\mathrm{g}} \simeq 2.5 r_{\mathrm{g}}$. The [S III] line luminosity is down by a factor of $10^{4/5} \sim 6.3$ from the value it would have had if it had been subthermal at r_{g}, rather than the factor of 10 drop at r_{g}, because most of the emission comes from further out where there is more volume.

The luminosity in the line will not linearly track $\Phi_{\rm EUV}$ because of the significant (and variable with $\Phi_{\rm EUV}$) collisional de-excitation of the transition. In fact, as long as $n_{\rm e}(r_{\rm g}, z_{\rm IF}) > n_{\rm ecr}$ and $f(S^{++})$is not dependent on$\Phi_{\rm EUV}$, the luminosity in the line scales as $\Phi_{\rm EUV}^{3/5}$ as shown in Equation (15). However, we find in our numerical analysis that $f(S^{++})$ does depend significantly on $\Phi_{\rm EUV}$, and the $\Phi_{\rm EUV}^{3/5}$ dependence is not seen (as we show below in our numerical models).

We have shown above that the fine structure emission from the H II surface region arises from $\sim r_{\rm g}$ as long as $n_{\rm e}(r_{\rm g}, z_{\rm IF}) < n_{\rm ecr}$. However, this conclusion and the important analytic derivation of the line luminosities (Equation (8)) both require that the surface H II region be ionization-bounded (i.e., there be a neutral layer underneath the completely ionized surface). The minimum mass of gas required to fully absorb the incident EUV photons and create an ionized surface region with a neutral midplane region for $r < r_{\rm g}$ is given as

$$M_{\rm H\,II}({\rm min}) = \int_{z_{\rm IF}}^{\infty} 2dz \int_0^{r_{\rm g}} m_{\rm H} n_{\rm e}(r, z) 2\pi r dr, \qquad (16)$$

where $m_{\rm H}$ is the mass of the ionized gas per electron ($\sim 2 \times 10^{-24}$ g). The z integral can be approximated as $2H(r) \equiv 2r_{\rm g}\left(\frac{r}{r_{\rm g}}\right)^{3/2}$ with the electron density fixed at the density at the ionization front $n_{\rm e}(r, z_{\rm IF})$. The density $n_{\rm e}(r, z_{\rm IF})$ falls as $r^{-3/2}$ for $r < r_{\rm g}$. Therefore, for $r < r_{\rm g}$ the mass is mostly at $r_{\rm g}$. Performing the integral, we obtain

$$M_{\rm H\,II}({\rm min}) \simeq 2\pi r_{\rm g}^3 m_{\rm H} n_{\rm e}(r_{\rm g}, z_{\rm IF}) \simeq 10^{-10} \left(\frac{\Phi_{\rm EUV}}{10^{41}\ {\rm s}^{-1}}\right)^{1/2} \times \left(\frac{M_*}{1\ M_\odot}\right)^{3/2} M_\odot. \qquad (17)$$

Thus, assuming $n_{\rm e}(r_{\rm g}) < n_{{\rm ecr},t}$, an extremely small gas mass, of order 10^{-7} Jupiter masses, inside of $r_{\rm g}$ will provide the luminosities given by Equation (8), using the values of C_t given in Table 1. These lines, then, are very sensitive diagnostics of the presence of trace amounts of gas at radii of order 1–10 AU in disks. If there is less mass than $M_{\rm H\,II}({\rm min})$ at $r_{\rm g}$, then the resulting luminosities will be reduced by a factor $M_{\rm H\,II}/M_{\rm H\,II}({\rm min})$.

We now address whether dust extinction is important in the H II surface region. Since $H(r) \propto r^{3/2}$, the 10^4 K surface of the disk is flared. Most of the emission comes from $r_{\rm g}$ or beyond as shown above. Using Equations (11) and (12), the attenuating column at $r_{\rm g}$ is roughly

$$N_{\rm att} \sim n_{\rm e}(r_{\rm g}, z_{\rm IF}) \times r_{\rm g} \sim 5 \times 10^{18} \left(\frac{\Phi_{\rm EUV}}{10^{41}\ {\rm s}^{-1}}\right)^{1/2} \times \left(\frac{1\ M_\odot}{M_*}\right)^{1/2} {\rm cm}^{-2}. \qquad (18)$$

The dust at the surface of the disk is expected to have less opacity than interstellar dust, so that the column for EUV optical depth unity is greater than 10^{21} cm^{-2}. The above equation shows that dust will not be important until $\Phi_{\rm EUV} > 10^{46}$ s^{-1} for a 1 $M_\odot$ star. Low-mass stars do not produce such high EUV luminosities. Therefore, our neglect of dust opacity in the H II surface is justified in disks around low-mass stars.

Finally, we estimate the fraction $f_{\rm EUV}$ of the ionizing photons emitted by the star that are absorbed by the disk. Most of the absorption (and consequent emission, as shown above) comes from $r \sim r_{\rm g}$ or beyond, and here $H \sim r$. As we will show below in our numerical disk models, the underlying neutral disk also has considerable height. At $r = 10$ AU, $z_{\rm IF} \simeq 7.5$ AU (see Section 4.2). Thus, the disk is opaque to EUV photons from the midplane to an angle from midplane of about 40°. In addition, the recombining hydrogen in the ionized gas above 40° also absorbs EUV photons. Therefore, we estimate that the fraction $f_{\rm EUV}$ of EUV photons absorbed by the disk is about 0.7. A detailed hydrodynamical study is needed to more accurately determine this fraction.

As our prime examples for this analytic analysis, consider specifically the case of the [Ne II] 12.8 μm, [Ne III] 15 μm, and [Ar II] 7 μm luminosity emerging from a young disk. We choose these lines because [Ne II] and [Ne III] have been observed, and [Ar II] is predicted to be the brightest of the unobserved lines (see Table 1). In addition, they all have high critical densities so that $n_{\rm e}(r_{\rm g}, z_{\rm IF}) < n_{\rm ecr}$ for these lines as long as $\Phi_{\rm EUV} < 10^{42}$–10^{43} s^{-1}. Assuming that this condition is met and substituting $f_{\rm EUV} = 0.7$ and the atomic constants into Equation (8), we obtain

$$L_{\rm [Ne\,II]} \simeq 3.8 \times 10^{-6} f({\rm Ne}^+) \left(\frac{\Phi_{\rm EUV}}{10^{41}\ {\rm s}^{-1}}\right) L_\odot. \qquad (19)$$

$$L_{\rm [Ne\,III]} \simeq 6.4 \times 10^{-6} f({\rm Ne}^{++}) \left(\frac{\Phi_{\rm EUV}}{10^{41}\ {\rm s}^{-1}}\right) L_\odot. \qquad (20)$$

$$L_{\rm [Ar\,II]} \simeq 3.2 \times 10^{-6} f({\rm Ar}^+) \left(\frac{\Phi_{\rm EUV}}{10^{41}\ {\rm s}^{-1}}\right) L_\odot. \qquad (21)$$

Recall that $f({\rm Ne}^+)$ is the fraction of neon in the singly ionized state in the region near $r_{\rm g}$ which produces most of the emission. Luminosities greater than about $10^{-7}\ L_\odot$ are detectable from nearby (< 100 pc) sources by the *Spitzer Space Telescope*, as long as the line-to-continuum ratio is sufficiently large to enable detection of the line above the bright continuum.

The effect on IR luminosity caused by holes in disks. The above analytic results apply for a disk that extends inward to $r \lesssim r_{\rm g} \sim 7$ AU from the star. However, disks have been observed with inner holes, devoid of dust, that extend to $r_{\rm i} > r_{\rm g}$ (e.g., Najita et al. 2007; Salyk et al. 2009). Regardless of the cause of these holes, if gas is absent inside of $r_{\rm i}$ and $r_{\rm i} > r_{\rm g}$, the disk vigorously photoevaporates at $r_{\rm i}$, a process which evaporates the disk from inside out (Alexander et al. 2006a, 2006b). Alexander et al. showed that the flux of EUV photons striking the inner wall of the disk creates a thin (thickness $\simeq H$, the scale height of the neutral disk at $r_{\rm i}$) ionized layer. The Strömgren condition gives the electron density in the layer:

$$F_{\rm EUV} \equiv \frac{\Phi_{\rm EUV}}{4\pi r_{\rm i}^2} = \alpha_{r,H} n_{\rm e}^2 H \qquad (22)$$

Assuming $H \simeq 0.1 r_{\rm i}$ (Alexander et al. 2006a, 2006b), we obtain

$$n_{\rm e}(r_{\rm i}) \simeq 2.5 \times 10^5 \left(\frac{\Phi_{\rm EUV}}{10^{41}\ {\rm s}^{-1}}\right)^{1/2} \left(\frac{10\ {\rm AU}}{r_{\rm i}}\right)^{3/2} {\rm cm}^{-3}. \qquad (23)$$

Note that the electron density decreases as the inner hole size increases. If $r_{\rm i} \gg r_{\rm g}$, this leads to an increase in the luminosity of low critical density lines with respect to high critical density lines (see Equation (8)). However, for lines whose critical densities are larger than the electron density at $r_{\rm g}$, the presence of a hole of size $r_{\rm i} \gg r_{\rm g}$ does not appreciably affect the IR line luminosity. Essentially, this arises because the IR line luminosity is proportional to the number of EUV

photons absorbed, $f_{\rm EUV}\Phi_{\rm EUV}$, and this remains constant, with $f_{\rm EUV} \sim 0.7$, regardless of $r_{\rm i}$. Therefore, the IR line luminosity tracks $\Phi_{\rm EUV}$ as presented in Equation (8).

3.2. Infrared Hydrogen Recombination Lines from the H II Surface

The IR hydrogen recombination lines can be analytically determined by noting that the luminosity in a given line produced by the transition n_u to n_l is given as

$$L_{ul} = \alpha_{ul}\Delta E_{ul}\int_{z_{\rm IF}}^{\infty} dz \int_{r_{\rm i}}^{r_{\rm o}} 2\pi r n_{\rm e}^2 dr, \tag{24}$$

where α_{ul} is the rate coefficient for recombinations through the n_u–n_l transition and ΔE_{ul} is the energy of the photon produced in this transition. Clearly, the hydrogen recombination lines also count EUV photons (see Equation (5)) and could be used to measure $\Phi_{\rm EUV}$. However, hydrogen recombination produces weak IR lines compared to the fine structure lines such as [Ne II] if the electron density $n_{\rm e}$ is less than the critical density $n_{\rm ecr}$ of the fine structure transition, as can be seen by taking the ratio of the predicted line luminosities:

$$\frac{L_{ul}}{L({\rm Ne\,II})} = \frac{\alpha_{ul}\Delta E_{ul}}{\gamma_{[{\rm Ne\,II}]}\Delta E_{{\rm Ne\,II}} x_{\rm Ne} f({\rm Ne}^+)}. \tag{25}$$

The hydrogen recombination lines we are most interested in are the 7–6 (Humphreys α) and 6–5 (Pfund α) at wavelengths of 12.37 and 7.46 μm, respectively. These two lines have been reported observed toward stars with disks (Pascucci et al. 2007; Ratzka et al. 2007). Substituting the atomic constants for these transitions, we obtain predicted ratios for the EUV-induced surface H II layer:

$$\frac{L_{7-6}}{L({\rm Ne\,II})} = 0.008 \tag{26}$$

and

$$\frac{L_{6-5}}{L({\rm Ne\,II})} = 0.02. \tag{27}$$

The observed ratios are close to unity! The predicted ratios are small because of the low ratio of the radiative recombination rate α_{ul} of hydrogen to the electronic collisional excitation rate of [Ne II] $\gamma_{[{\rm Ne\,II}]}$. Thus, we predict that these IR hydrogen recombination lines must originate from another source if [Ne II] originates from the H II region surface of the disk. One place which would provide copious recombination line emission without producing even more [Ne II] emission would be very high electron density regions, $n_{\rm e} \gg n_{{\rm ecr},[{\rm Ne\,II}]}$. In these regions, [Ne II] is suppressed relative to the hydrogen recombination lines due to the collisional de-excitation of the upper level of the [Ne II] transition. Therefore, these observed recombination lines are possibly produced in very dense plasma very close to the star, in the stellar chromosphere, the accretion shock, or an internal wind shock if it is both high speed ($v_s \gtrsim 100$ km s^{-1} so that it produces ionized hydrogen) and occurs so close to the wind origin ($\lesssim$1 AU) that the postshock density is high enough to suppress [Ne II] relative to the recombination lines. In any of these cases, the prediction is that the H recombination lines will be much broader ($\gtrsim$100 km s^{-1}) than the [Ne II] lines ($\sim$20 km s^{-1}) in face-on disks.

3.3. Infrared Fine Structure Lines from the X-ray-heated and Ionized Subsurface Layer

Glassgold et al. (2007) and Meijerink et al. (2008) have presented models of the [Ne II] 12.8 μm emission and emission from other lines, such as [Ne III], [O I], [S III], and [S IV], produced in the X-ray-heated layer that lies just below the ionization front created by EUV photons. This layer is predominately neutral, $x_e \sim 0.001$–0.1, depending on r and z, but with a higher ratio of Ne$^+$/Ne. Typically, the [Ne II] emitting layer has $T \sim 1000$–4000 K. In Section 4, we also present numerical results from our models of the X-ray-induced fine structure emission, and in Section 5 we discuss differences between our models and those of these authors. Here, we present a simple analytic estimate of the strengths of the fine structure transitions in X-ray-illuminated regions. These estimates are more approximate than those presented above for the EUV-dominated regions because of the uncertainties in estimating the gas temperature in this mostly neutral gas illuminated by a spectrum of X-ray photons. Nevertheless, they provide insight into the X-ray process and into the relative strengths of X-ray-induced fine structure emission in the X-ray layer as opposed to that produced by EUV photons in the surface EUV layer.

The simplest derivation arises if we assume our "hard" X-ray spectrum, dominated by 1–2 keV photons. These photons are sufficiently energetic to ionize the K shell of Ne, and the ionization of Ne is dominated by direct X-ray photoabsorption, and not by collisions with secondary electrons. If we make the assumption in the X-ray layer that the atomic Ne absorbs a fraction $f_{\rm Ne}^X$ of all $\sim$1 keV X-rays and that Ne$^+$ radiatively recombines with electrons, and we assume that $n_{\rm e} < n_{{\rm ecr},[{\rm Ne\,II}]}$, we obtain in a manner completely analogous to the EUV layer's Equations (5)–(7)

$$L^X_{[{\rm Ne\,II}]} = \frac{\gamma^X_{[{\rm Ne\,II}]}\Delta E_{[{\rm Ne\,II}]} f^X_{\rm Ne} f_X \Phi_X}{2\alpha_{r,{\rm Ne}}}. \tag{28}$$

Here, $\gamma^X_{[{\rm Ne\,II}]}$ is the collisional rate coefficient for [Ne II] by electrons in the X-ray layer (i.e., it is only different from $\gamma_{[{\rm Ne\,II}]}$ in Equation (7) because the X-ray layer is cooler than the EUV layer), Φ_X is the $\sim$1 keV X-ray photon luminosity of the central source, f_X is the fraction of X-rays absorbed by the disk in the X-ray layer, and $\alpha_{r,{\rm Ne}}$ is the recombination rate coefficient of Ne$^+$ with electrons in the X-ray layer. The fraction of $\sim$1 keV photons absorbed by neon, $f^X_{\rm Ne}$, is approximately the neon cross section at 1 keV divided by the total X-ray absorption cross section at 1 keV; using Wilms et al. (2000), we obtain $f^X_{\rm Ne} \simeq 0.21$. We see that $L^X_{[{\rm Ne\,II}]}$ scales linearly with Φ_X, just as $L_{[{\rm Ne\,II}]}$ scales linearly with $\Phi_{\rm EUV}$ in the EUV layer. The ratio of the [Ne II] luminosity from the EUV layer to that in the X-ray layer is then given as

$$\frac{L_{[{\rm Ne\,II}]}}{L^X_{[{\rm Ne\,II}]}} = \left(\frac{\gamma_{[{\rm Ne\,II}]}}{\gamma^X_{[{\rm Ne\,II}]}}\right)\left(\frac{f_{\rm EUV}}{f^X_{\rm Ne} f_X}\right)\left(\frac{\alpha_{r,Ne}}{\alpha_{r,H}}\right)\left(\frac{\Phi_{\rm EUV}}{\Phi_X}\right) x_{\rm Ne} f({\rm Ne}^+), \tag{29}$$

where $f({\rm Ne}^+)$ is the fraction of neon that is singly ionized in the EUV layer. We take $T \sim 10^4$ K for the EUV layer and $T_X \sim 2000$ K for the X-ray layer to estimate the recombination coefficients, and assuming that f_X is approximately the height of the layer which becomes optically thin to 1 keV X-rays from the star (roughly $N \sim 10^{21}$ cm^{-2}, or a column of about 10^{22} to the star) divided by r or $f_X \sim 0.25$ (see Figure 5). The EUV layer is more flared; hence $f_{\rm EUV} \sim 0.7$. In the EUV layer, $f({\rm Ne}^+) \simeq 1$.

Substituting into Equation (29), we obtain

$$\frac{L_{[\mathrm{Ne\,II}]}}{L^X_{[\mathrm{Ne\,II}]}} \simeq 2\times10^{-3} e^{\frac{1100\ \mathrm{K}}{T_X}} \left(\frac{\Phi_{\mathrm{EUV}}}{\Phi_X}\right). \quad (30)$$

The 1 keV X-ray photon luminosity Φ_X from a typical source is of order 10^{39} photons s^{-1}. The EUV luminosity Φ_{EUV} is generally of order 10^{41} photons s^{-1}. Therefore, assuming that the 1 keV X-rays are absorbed in regions with $T_X > 1000$ K, the [Ne II] luminosity is expected to be marginally dominated by emission from the X-ray layer as opposed to the EUV layer. We show below in our numerical work that $L_{[\mathrm{Ne\,II}]}/L^X_{[\mathrm{Ne\,II}]} \sim 0.6$ when $\Phi_{\mathrm{EUV}} = 10^{41}$ s^{-1} and $\Phi_X \simeq 10^{39}$ s^{-1} and when the EUV spectrum is such to produce more Ne^+ than Ne^{++} in the EUV layer; this result agrees with Equation (30). Note that $\Phi_{\mathrm{EUV}} = 10^{41}$ s^{-1} and $\Phi_X \simeq 10^{39}$ s^{-1} corresponds to $L_{\mathrm{EUV}} \simeq L_X$. In other words, if the central star emits the same EUV and X-ray luminosity, and the EUV has a soft spectrum which produces more [Ne II] than [Ne III], there will be roughly 2 times more [Ne II] luminosity arising from the X-ray layer than from the EUV layer. As we will show in Section 4, where we present results from our detailed numerical models, this conclusion that *X-rays are more efficient at producing* [Ne II] *emission* does not depend strongly on the X-ray spectrum for reasonable choices of the spectrum. If we adopt a softer spectrum, the ionization of Ne is dominated by secondary electrons because most of the X-rays are absorbed by He, C, or O. The gas is also hotter because there is more heating per unit volume due to the higher cross sections for softer X-rays. The net effect is that the [Ne II] luminosity does not change much for fixed X-ray luminosity even as we vary the X-ray spectrum. In the case of the "hard" X-ray spectrum, the reason X-rays are somewhat more dominant than the EUV is because for high temperature ($T > 1000$ K) gas such as exist in both the H II region and the X-ray-heated region, the luminosity in the line depends mainly on the number of Ne^+ ions times the electron density. In the H II region, the vast number of EUV photons are used ionizing H, an extremely small fraction of the photons are used ionizing Ne, and therefore the number of Ne^+ ions times the electron density is a small (the $x_{\mathrm{Ne}} f(\mathrm{Ne}^+)$ factor in Equation (29); however, we explicitly include the relatively large fraction, $f^X_{\mathrm{Ne}} = 0.21$ of 1 keV X-ray photons that directly ionize Ne and lead to a large product of electron density times Ne^+ ions in Equation (29). Therefore, no $x_{\mathrm{Ne}} f(\mathrm{Ne}^+)$ term appears in the denominator. Another way of understanding this result is that although the EUV layer is completely ionized with $f(\mathrm{Ne}^+) \sim 1$ and $x_e \sim 1$, the EUV layer has much less column of Ne^+ because H and He rapidly absorb the EUV photons; the penetrating X-rays partially ionize a much larger column.

3.4. Shock Origin of Ionized Infrared Fine Structure Lines

Lahuis et al. (2007) and van Boekel et al. (2009) discussed the possible origin of [Ne II] emission from shocks generated by protostellar outflows. In order for a shock to produce significant [Ne II] emission, the shock must ionize most of the preshock gas in order to produce high quantities of Ne^+ and electrons. The fraction of preshock gas that is ionized by the shock is a very sensitive function of the shock speed v_s (e.g., Hollenbach & McKee 1989, hereafter HM89). HM89 showed that $v_s \gtrsim 100$ km s^{-1} is required to ionize most of the H and Ne and that the [Ne II] emission rises very sharply with v_s and then plateaus above $v_s \gtrsim 100$ km s^{-1}. This suggests that any possible shock must originate from internal shocks in the protostellar wind (which has terminal speeds of ~200 km s^{-1}) or from the protostellar wind overtaking much slower moving outflow material. It is unlikely to originate from the shock produced by the wind striking the disk, since this shock is so oblique that the (normal) shock speeds are typically $\lesssim$20 km s^{-1} (Matsuyama et al. 2009). The total emission per unit area F_t from the postshock region of a radiative shock is given as

$$F_t = \frac{1}{2} m_{\mathrm{H}} n_0 v_s^3, \quad (31)$$

where m_{H} is the mass per hydrogen nucleus and n_0 is the hydrogen nucleus number density of the preshock gas. The numerical results of HM89 can be approximated for the emission per unit area of [Ne II] for shocks with $v_s \gtrsim 100$ km s^{-1}:

$$F_{[\mathrm{Ne\,II}]} \simeq \left(\frac{5\times10^{-3}}{1+\frac{n_0}{10^4\ \mathrm{cm}^{-3}}}\right) F_t, \quad (32)$$

where the dependence on density at high density arises because of collisional de-excitation of the upper state of [Ne II] in the postshock gas. Assume that a fraction f_{sh} of the protostellar wind shocks at speeds $v_s \sim 100$ km s^{-1} with preshock density n_0. It follows that the [Ne II] shock luminosity is

$$L^{sh}_{[\mathrm{Ne\,II}]} = \frac{1}{2} f_{\mathrm{sh}} \dot{M}_{\mathrm{w}} v_s^2 \left(\frac{5\times10^{-3}}{1+\frac{n_0}{10^4\ \mathrm{cm}^{-3}}}\right)$$
$$\simeq \left(\frac{4\times10^{-5}}{1+\frac{n_0}{10^4\ \mathrm{cm}^{-3}}}\right) f_{\mathrm{sh}} \dot{M}_{-8}\ L_\odot, \quad (33)$$

where $\dot{M}_{-8} = \dot{M}_{\mathrm{w}}/10^{-8}\,M_\odot$ yr^{-1} and $v_s \gtrsim 100$ km s^{-1}. Therefore, if the protostellar wind mass loss rate $\dot{M}_{\mathrm{w}} \gtrsim 10^{-9}\,M_\odot$ yr^{-1}, $v_s \gtrsim 100$ km s^{-1}, $f_{\mathrm{sh}} \sim 1$, and $n_0 \lesssim 10^4$ cm^{-3}, then the [Ne II] luminosity produced in internal wind shocks may be comparable to or greater than the luminosity produced in the EUV or X-ray layer of the disk.

Van Boekel et al. (2009) argued this may be the case in T Tau S. Here, the observed [Ne II] luminosity is $L_{[\mathrm{Ne\,II}]} \sim 10^{-3}\,L_\odot$. From the above, this would require, for example, $f_{\mathrm{sh}} \sim 1$, $\dot{M}_{\mathrm{w}} \sim 2.5\times10^{-7}\,M_\odot$ yr^{-1}, and $n_0 \lesssim 10^4$ cm^{-3}. The preshock density can be estimated with knowledge of the distance of the shock from the star, r_{sh}, and $\dot{M}_{\mathrm{w}}$. The preshock density (the density in the wind at r_{sh}) is given as

$$n_0 = 2.5\times10^3 \dot{M}_{-8}\, r_{15}^{-2} f_\Omega^{-1}\ \mathrm{cm}^{-3}, \quad (34)$$

where $r_{15} = r_{\mathrm{sh}}/10^{15}$ cm and f_Ω is the fraction of 4π steradians into which the protostellar wind is collimated. Van Boekel et al. (2009) measured an extent of the emission from T Tau S of approximately 160 AU. If we assume $r_{\mathrm{sh}} = 160$ AU and $f_\Omega = 1$, presumably upper limits, we obtain a lower limit to $n_0 \gtrsim 1.5\times10^4$ cm^{-3}. Note that for $\dot{M}_{\mathrm{w}} > 2.5\times10^{-7}\,M_\odot$ yr^{-1} and for our specific assumptions on r_{sh} and f_Ω, the preshock density is so high that the [Ne II] luminosity is independent of $\dot{M}_{\mathrm{w}}$; the luminosity from the shock saturates once the emitting [Ne II] in the postshock gas is in local thermodynamic equilibrium (LTE). Therefore, although it pushes parameters a bit uncomfortably, if T Tau S has protostellar mass loss rates $\gtrsim 2.5\times10^{-7}\,M_\odot$ yr^{-1}, it is possible that internal wind shocks produce the observed [Ne II] luminosity. Note that the "dynamical time," $v_s/r_{\mathrm{sh}} \sim 10$ yr, is marginally consistent with the observations of no significant time dependence since 1998 (van Boekel et al. 2009).

More recently, Güdel et al. (2009) have assembled [Ne II] data from a large number of sources and have plotted $L_{[\mathrm{Ne\,II}]}$ versus $\dot{M}_{\rm acc}$. For low values of $\dot{M}_{\rm acc} \lesssim 10^{-8}\ M_\odot\ \mathrm{yr}^{-1}$ the [Ne II] luminosity is nearly independent of $\dot{M}_{\rm acc}$, and is typically of order $3 \times 10^{-6}\ L_\odot$. However, for higher mass accretion rates and, in particular, for all the sources with known outflows or jets, $L_{[\mathrm{Ne\,II}]}$ increases with increasing $\dot{M}_{\rm acc}$ (arguably linearly, but with a lot of scatter). We present these observational results from Güdel et al. and compare them to Equation (33) in Section 4.4. The correlation of $L_{[\mathrm{Ne\,II}]}$ with $\dot{M}_{\rm acc}$ suggests that either the higher luminosity ($L_{[\mathrm{Ne\,II}]} \sim 10^{-5}$–$10^{-3}\ L_\odot$) sources may originate in protostellar shocks or from EUV or soft X-rays produced by the accretion of disk material onto the star. However, in the latter case, these photons must penetrate the disk wind, which seems unlikely.

3.5. [O I] 6300 Å Emission from Young Stars with Disks

[O I] 6300 Å emission is often observed in young low-mass stars with disks and outflows (e.g., Hartigan et al. 1995). Two velocity components are seen: a high velocity component "HVC" and a low velocity component "LVC." Hartigan et al. argued that the HVC comes from shocks in the protostellar wind, similar to our above discussion of internal shocks. The typical velocity of this component is ∼100–200 km s^{-1} and the [O I] 6300 Å luminosity is $\sim 10^{-6}$–$10^{-2}\ L_\odot$. HM89 showed that for $v_s \sim 100$ km s^{-1} the [O I] 6300 Å emission from the shock is about 10 times more luminous than the [Ne II] 12.8 μm emission for $n_0 \lesssim 10^4$ cm^{-3}, with even higher ratios at $n_0 > 10^4$ cm^{-3} because [O I] 6300 Å does not collisionally de-excite as readily as [Ne II] 12.8 μm. Therefore, in agreement with Hartigan et al, we find that mass outflow rates of $\gtrsim 10^{-7} M_\odot$ yr^{-1} can produce the most luminous [O I] 6300 Å HVC sources (see Equation (33)).

Hartigan et al. (1995) attributed the LVC to [O I] emission emanating from the disk surface, probably in a relatively slow outflow since the emission is observed to be slightly blueshifted (∼−5 km s^{-1} with great dispersion). However, there are red and blue wings extending to ±60 km s^{-1} in the LVC, presumably due to a combination of Keplerian rotation and outflow. The [O I] 6300 Å luminosity in the LVC ranges from $\sim 10^{-6}$ to $\sim 10^{-3}\ L_\odot$, with "typical" values of $\sim 10^{-4} L_\odot$ (Hartigan et al. 1995). The exact origin of the LVC [O I] emission, and its heating source, remains a mystery. In Section 4, we present our numerical model results for [O I] emission from the EUV layer and the X-ray layer. In agreement with previous work by Font et al. (2004), we find that the EUV layer can only provide [O I] 6300 Å luminosities $\lesssim 10^{-6}\ L_\odot$. Meijerink et al. (2008) were able to produce [O I] luminosities as high as $5 \times 10^{-5}\ L_\odot$ in their models of the X-ray layer. Therefore, they found it very difficult to explain the most luminous [O I] LVC sources, but were able to produce luminosities in accordance with many of the observations. However, our more detailed models with an X-ray spectrum similar to that assumed by Meijerink et al. produce lower [O I] luminosities, primarily because we obtain lower gas temperatures in the X-ray-heated layer (see below). However, if we use a softer X-ray spectrum such as the one proposed by Ercolano et al. (2009), we do obtain luminosities of order $10^{-4}\ L_\odot$. In summary, it appears that emission from the EUV and X-ray layers can only explain the lower and typical luminosity LVCs, but not the highest luminosity LVCs.

It is instructive to estimate what physical conditions are required to produce [O I] luminosities in the LVC as high as 10^{-4}–$10^{-3}\ L_\odot$. Consider a layer on the disk surface of thickness ℓ, temperature T, and extending to radius $r_{\rm o}$ from which most of the [O I] emanates. This top and bottom layer of the disk has hydrogen nucleus density n and vertical column N. Because the [O I] 6300 Å transition is $\Delta E/k = 23{,}000$ K above the ground state, we require $T \gtrsim$ several thousand degrees K for significant emission. The emerging [O I] 6300 Å luminosity produced by the surface layers is then given as

$$L_{[\mathrm{O\,I}]} = \pi r_{\rm o}^2 n_{\rm e} n(O) \gamma_{[\mathrm{O\,I}]} \ell, \tag{35}$$

where $\gamma_{[\mathrm{O\,I}]}$ is the collisional excitation rate for electrons on atomic oxygen, $n(O)$ is the density of atomic oxygen, and $n_{\rm e}$ is the electron density. We account here for both the top and bottom of the disk, but recall that half of the luminosity (that directed to the midplane) is absorbed by the optically thick disk. Equation (35) assumes $n_{\rm e}$ to be less than the critical density $n_{\rm ecr}$. (HM89 gave $n_{\rm ecr} \sim 10^6$ cm^{-3}, so $n_{\rm e} < n_{\rm ecr}$ is generally satisfied.) HM89 gave $\gamma_{[\mathrm{O\,I}]} = 8.5 \times 10^{-9} T_4^{0.57} e^{-2.3/T_4}$ cm^3 s^{-1}, with $T_4 = T/10^4$ K. Oxygen rapidly charge exchanges with hydrogen and therefore at high temperatures ($T \gg 200$ K) $\mathrm{O^+/O} = \mathrm{H^+/H}$. Therefore, $n_{\rm e} = x_e n$ and $n(\mathrm{O}) = x(H) n_{\rm O}$, where $n_{\rm O} \simeq 3 \times 10^{-4} n$ is the gas phase density of oxygen in both O and $\mathrm{O^+}$ and $x(H)$ is the abundance of atomic hydrogen. It follows that

$$L_{[\mathrm{O\,I}]} \simeq 6.5 \times 10^{-4} x_e x(H) n_5 r_{14}^2 N_{20} T_4^{0.57} e^{-2.3/T_4}\ L_\odot, \tag{36}$$

where $r_{14} = r_{\rm o}/10^{14}$ cm, $n_5 = n/10^5$ cm^{-3}, and $N_{20} = N/10^{20}$ cm^{-2}. This analytic exercise shows that to produce $L_{[\mathrm{O\,I}]} \sim 10^{-4}$–$10^3\ L_\odot$ in the LVC requires, for example, surface layers with $n \sim 10^5$cm^{-3}, $N \sim 10^{20}$ cm^{-2}, $r_{\rm o} \sim 60$ AU, $T \sim 10^4$ K, and $x_e \sim 0.5$. In the EUV layer $x_e \sim 1$, $T_4 \sim 1$, and $r_{14}^2 \sim 1$ (recall that most of emission arises from $r \sim r_{\rm g}$). Therefore, the [O I] luminosity from the EUV layer is approximately

$$L'_{[\mathrm{O\,I}]} \simeq 6.5 \times 10^{-5} x(H) r_{14}^2 n_5 N_{20}\ L_\odot. \tag{37}$$

This equation shows the difficulty in producing the observed [O I] emission from the EUV layer: the fraction of neutral gas $x(H)$ is very low in the EUV layer or, equivalently, the fraction of atomic oxygen is very low. In addition, the emission mostly arises from $r \sim r_{\rm g} \sim 10^{14}$ cm, which is not large, and $n_5 N_{20}$ rarely exceeds unity.

On the other hand, in the X-ray layer the temperature is of order $T_4 \sim 0.1$–0.4 and $x(H) \sim 1$ so that

$$L^X_{[\mathrm{O\,I}]} \simeq 6.5 \times 10^{-4} x_e n_5 r_{14}^2 N_{20} T_4^{0.57} e^{-2.3/T_4}\ L_\odot. \tag{38}$$

The X-ray layer has $x_e \lesssim 0.1$, $r_{14}^2 \lesssim 10$, $n_5 \lesssim 100$, and $N_{20} \lesssim 10$. Even inserting these upper limits, we find that the [O I] luminosity is at most $10^{-3}\ L_\odot$ if $T = 4000$ K and $3 \times 10^{-6} L_\odot$ if $T = 2000$ K. Therefore, the [O I] luminosity is extremely sensitive to the gas temperature (and its variation in r and z) in the X-ray layer. The Meijerink et al. (2008) model has high temperatures, ∼3000–4000 K, in the X-ray layer out to 10–20 AU in their case with a relatively high X-ray luminosity of 2×10^{31} erg s^{-1}. For this case, they therefore find $L^X_{[\mathrm{O\,I}]} \sim 5 \times 10^{-5}\ L_\odot$. Our model for the same case, however, gets temperatures in the X-ray layer in the range 1500–2500 K, and therefore we get an [O I] luminosity of only $\sim 5 \times 10^{-7}\ L_\odot$ (see Section 4.4). However, keeping the X-ray luminosity the same but assuming a much softer power-law spectrum ($L(E) \propto E^{-1}$ from 0.1 to 2 keV), we do find that the X-ray-heated gas becomes

hotter and the [O I] luminosities approach $10^{-4}\ L_\odot$. We discuss in Section 4.3 the reasons for the differences in temperature in our model relative to that of Meijerink et al. We conclude that it is unlikely that the X-ray layer can provide the highest [O I] luminosities observed in some LVC sources, but that soft X-ray sources can produce the typical luminosities.

The "transition layer" ($x_e \sim 0.5$) between the fully ionized EUV layer and the partially ionized X-ray layer is also unlikely to produce either the highest observed [O I] luminosities or even the typical luminosities. The density in this layer is similar to the density at the base of the EUV layer, or $n \sim 10^5 \Phi_{41}^{1/2}$ cm^{-3} at $r = r_g = 7$ AU (see Equation (12)). However, beyond $r_g = 7$ AU the density falls as $r^{-5/2}$ so that most of the emission arises from $r \sim 7$ AU. In addition, the column N of this transition layer is roughly the column for optical depth unity in EUV photons, or $N \sim 10^{18}$ cm^{-2}. Therefore, the small r_0 and low N conspire to produce only $L_{[O\,I]} \sim 10^{-6}\ L_\odot$.

We plan to investigate the possibility that the source of the LVC arises from the shear layer produced when the protostellar wind strikes the surface of the disk obliquely and sets up an outward moving layer of shocked wind and entrained disk surface gas (a "shear" layer; see Matsuyama et al. 2009, hereafter MJH09). MJH09 showed that this layer can have columns $N \sim 10^{19}$–10^{20} cm^{-2} out to 100 AU. As noted earlier, the oblique wind shock ($v_s \lesssim 20$ km s^{-1}) is insufficient to ionize hydrogen or helium to provide the electrons needed for [O I] excitation. Therefore, we require the EUV and soft X-rays to ionize this layer. This shear layer is likely turbulent so that there may be rapid mixing of the bottom (cooler and more neutral layers) with the top shear layers, perhaps allowing $x_e \sim 0.5$ and $x(H) \sim 0.5$ in the entire layer (the most efficient for producing [O I]) and maintaining a relatively isothermal layer. The heating would be a combination of shock/turbulent heating plus the heating due to photoionization by EUV and soft X-rays. The density n in the shear layer (MJH09) is approximately $n \sim 3000\, \dot{M}_{-8} r_{15}^{-2}$ cm^{-3}. Note that we cannot allow $\dot{M}_{-8}$ to exceed unity or the EUV and soft X-rays will not be able to penetrate the base of the wind to heat and ionize the shear layer. Therefore, although the shear layer may provide sufficient column N, electron fraction x_e, and temperature T, it appears unlikely to produce sufficient nr^2 to give the observed [O I] luminosities in the more luminous sources. Further work is needed to confirm this rough argument.

We conclude that the origin of the very luminous LVC [O I] emission is not from the EUV layer, the X-ray layer, or the transition layer. The typical LVC [O I] emission, however, may be produced by soft X-rays. The LVCs are also unlikely to originate from the shear layer set up by the impact of the protostellar wind. Perhaps a model that invokes ambipolar diffusion as a heating source, such as those that Safier (1993a, 1993b) has constructed for the HVC, might be applicable for the most luminous LVCs. However, the EUV layer is capable of producing the lowest luminosity sources, and the X-ray layer may produce the typical luminosity, so we proceed with detailed numerical studies of the [O I] luminosity from these layers in Section 4.

4. NUMERICAL MODEL AND RESULTS

4.1. The Extreme Ultraviolet Surface Layer and the Underlying X-ray Layer

Gorti & Hollenbach (2008) described the numerical code that we use to calculate, self-consistently, the gas temperature, gas density, and chemical structure of the predominantly neutral gas in the disk. To summarize, the code includes ~600 reactions among 84 species, gas heating by a number of mechanisms including FUV grain/polycyclic aromatic hydrocarbon (PAH) photoelectric heating and the heating caused by X-ray ionization of the gas, and cooling not only from collisional excitation of the species followed by radiative decay, but also from gas–grain collisions when the dust is colder than the gas. In some instances, for example, deep in the disk below the surface layers, the dust is warmer than the gas in which case gas–grain collisions can be an important heating source for the gas. The vertical structure of the disk is calculated self-consistently by using the computed gas temperature and density to calculate the thermal pressure and then balancing thermal pressure gradients with the vertical (downward) gravitational force from the central star.

For this paper we consider the "chemistry" of the fully ionized (H II) surface region, photoionized by the EUV radiation field from the star. By "chemistry," we mean the computation of the different ionic states of a given element by balancing photoionization with electronic recombination and charge exchange reactions. Photoionization rates are computed using cross sections from Verner et al. (1996). Recombination rates are taken from Aldrovandi & Pequignot (1973), Shull & van Steenberg (1982), and Arnaud & Rothenflug (1985). Charge exchange rates are from Kingdon & Ferland (1996). We assume a gas temperature of 10^4 K and do not perform thermal balance calculations in the H II region. In short, our code for the surface of the disk is an H II region code where we assume an EUV spectrum from the central star and then compute the abundances of, for example, Ne^+, Ne^{++}, and Ne^{+++} at each point r, z in the surface H II region. At each point r, z, we compute both the direct EUV flux from the star and the diffuse EUV field caused by recombinations to the ground state of atomic hydrogen in the surface H II region. We use the method described by Hollenbach et al. (1994) and utilized by Font et al. (2004) to do both these computations. The code finds the electron density $n_e(r, z_{IF})$ at the base of the surface H II region (in other words, at the ionization front separating the ionized surface from the predominantly neutral disk below). The thermal pressure at the IF is then $P_{IF} \simeq 2n_e(r, z_{IF})kT_{II}$, where $T_{II} = 10^4$ K and the factor of 2 includes the pressure from protons, He^+, and electrons. This pressure then determines the height z_{IF} where the thermal pressure in the predominantly neutral gas has dropped from its midplane value to P_{IF}. The parameter z_{IF} is the height of the base of the H II region: above z_{IF} the emission is mostly EUV-induced and we call this region the EUV surface layer; below z_{IF} the emission is mostly X-ray-induced and we call this region the X-ray layer.[3]

Implicit in our model is the assumption that the EUV luminosity and the X-ray luminosity are generated close to the stellar surface. This assumption then allows us to determine the column density of wind that the EUV and X-ray fluxes must traverse (see Section 2) as well as the angle of incidence of the EUV and X-ray flux on the flared disk surface. Since we assume that the protostellar disk wind originates near $r \sim 10^{12}$ cm, our estimate of the attenuation column density at the wind base is valid as long as the EUV and X-ray source of luminosity originates roughly within this distance from the stellar surface. Models of X-ray flares indicate that the X-rays probably arise from flares whose size ranges from 0.1 to 10 times the stellar

[3] We note that FUV may contribute to the heating in the X-ray layer. However, X-rays produce Ne^+ and the electrons necessary for efficient excitation of [Ne II] and [O I]. Therefore, it is proper to call this the "X-ray layer."

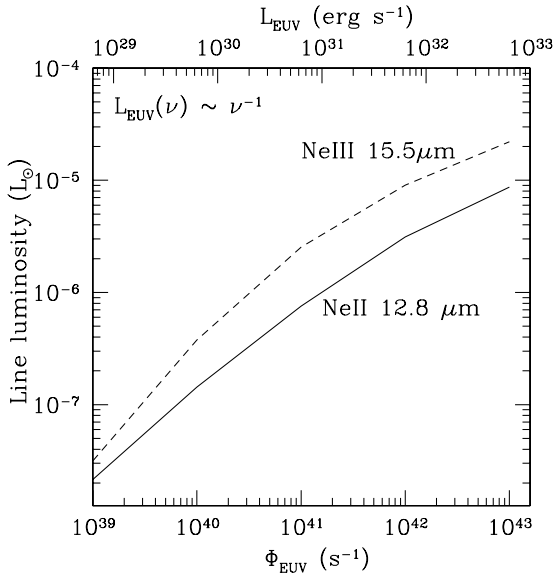

Figure 1. Dependence of [Ne II] 12.8 μm and [Ne III] 15.5 μm luminosity on the EUV luminosity (top in erg s^{-1} and bottom in EUV photons s^{-1}) of the central star. The EUV spectrum is assumed to be a power law, $L_{\rm EUV}(\nu) \propto \nu^{-1}$. This relatively hard EUV spectrum leads to high abundances of Ne^{++} in the EUV layer and [Ne III] stronger than [Ne II]. In Section 3, we explain the overall dependence of the line luminosity proportional to EUV luminosity with saturation occurring at the higher luminosities as electron densities exceed the critical density of the [Ne II] and [Ne III] transitions.

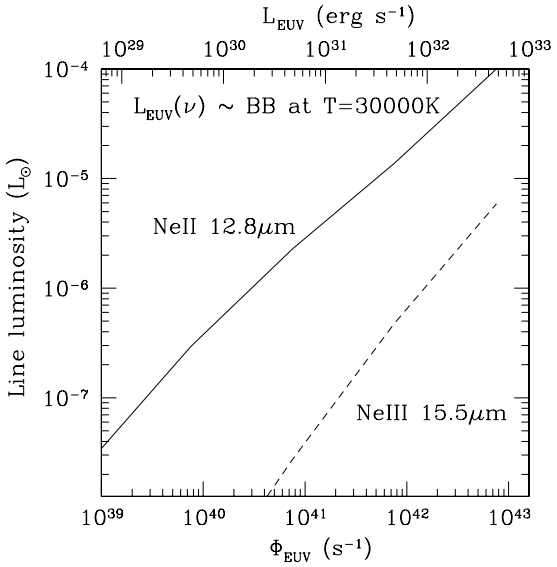

Figure 2. Dependence of [Ne II] 12.8 μm and [Ne III] 15.5 μm luminosity on the EUV luminosity (top in erg s^{-1} and bottom in EUV photons s^{-1}) of the central star. The EUV spectrum is assumed to be a blackbody with effective temperature $T_{\rm eff}$ = 30,000 K. This relatively soft EUV spectrum leads to high abundances of Ne^{+} in the EUV layer and [Ne II] significantly stronger than [Ne III]. In Section 3, we explain the overall dependence of the line luminosity proportional to the EUV luminosity.

radius (e.g., Favata et al. 2001, 2005; Grosso et al. 2004; Franciosini et al. 2007; Stelzer et al. 2007; Getman et al. 2008a, 2008b). Therefore, our estimate of the attenuation column is likely valid. Similarly, the line emission that we model usually arises from $r \sim$ 1–10 AU in the disk, and so the placement of the EUV or X-ray source within 10^{12} cm of the star does not affect our results. However, in DG Tau, a soft X-ray source has been imaged and seen to arise about 20 AU from the star, probably from shocks in a jet (Güdel et al. 2008; Schneider & Schmitt 2008). Such a geometry would certainly lower the column of attenuating wind, because of the spherical divergence of the wind. In addition, the X-ray flux would strike the disk from above, nearly normal to the surface. This latter effect, however, will likely not significantly affect the luminosities in the lines, since as we have shown in Section 3, the line luminosities are really an emission measure effect, and mainly depend on the fraction of energetic photons that the disk absorbs. If the source is 20 AU from the star, roughly half of the energetic photons are absorbed. We show below that in the case of a flared disk with a central source of energetic photons, nearly 0.7 of the photons are absorbed. Therefore, the fraction of photons absorbed is nearly the same.

Also implicit in our model is that the X-ray luminosity is the mean value of the time variable X-ray luminosity. Getman et al. (2008a) showed that typical decay times of flares is of the order of hours to days. In the EUV and X-ray layers where the modeled lines originate, recombination and cooling timescales are of the order of 1–10 yr. Thus, the gas generally does not have time to respond to the flares, but settles to a state given by the mean value of the X-ray luminosity.

4.2. The Extreme Ultraviolet Layer Results

Figures 1 and 2 show the results of models as we vary the EUV luminosity. We assume two forms for the EUV spectrum. The first form (Figure 1) is a relatively hard spectrum; we assume a power-law spectrum νL_ν = constant from 13.6 eV to the X-ray regime (~0.1 keV). This spectrum is motivated by the fact that νL_ν in the FUV band is observed to be similar to νL_ν in the X-ray band, and each band typically has $\nu L_\nu \sim 10^{-3}\, L_*$, where L_* is the stellar bolometric luminosity. On the other hand, the EUV spectrum is very uncertain. The Ribas et al. (2005) observations of older, but very nearby, solar mass stars show EUV spectra, which can drop rapidly from 13.6 eV to 40 eV, even though the overall trend from the FUV to the X-ray tends to roughly an $L_\nu \propto \nu^{-1}$ spectrum. To simulate a softer spectrum than the first form, we take a blackbody spectrum with an effective temperature of 30,000 K (Figure 2). We are further motivated to adopt a softer spectrum by the observations in one source of the ratio [Ne III] 15 μm/[Ne II] 12.8 μm $\lesssim$ 0.06 (Lahuis et al. 2007) and because [Ne II] has been detected in more than 25 sources and none of them show [Ne III]. Our first form of the EUV spectrum produces a ratio > 1! This either indicates very little production of [Ne II] by the EUV layer or the fact that the EUV spectrum is much softer. We therefore have chosen a blackbody EUV spectrum that provides ratios in accord with measured values or upper limits on the ratio.

Figures 1 and 2 show the nearly linear rise in $L_{\rm [Ne\,II]}$ or $L_{\rm [Ne\,III]}$ with $L_{\rm EUV}$ as predicted in Equations (19) and (20). The absolute values are also in good agreement with these equations. At very high $L_{\rm EUV}$ this linear relationship breaks down for [Ne III], and $L_{\rm Ne\,III}$ begin to saturate because the electron densities in the dominant emitting regions begin to exceed $n_{\rm ecr,[Ne\,III]}$. For our power-law spectrum in Figure 1, we find that by fitting our analytic results to the model, $f(Ne^{++}) \sim 0.75$ and $f(Ne^{+}) \sim 0.25$, that is, 75% of the emitting neon is in Ne^{++} and only 25% in Ne^{+}. However, in Figure 2 we see that a softer EUV spectrum (blackbody with $T_{\rm eff}$ = 30,000 K) will reverse the situation so that [Ne II] dominates. Another mechanism, not treated here, that would quench [Ne III] and raise [Ne II] would be turbulent mixing of neutral gas into the H II region. The charge exchange reaction $Ne^{++} + H \rightarrow Ne^{+} + H^{+}$ is very

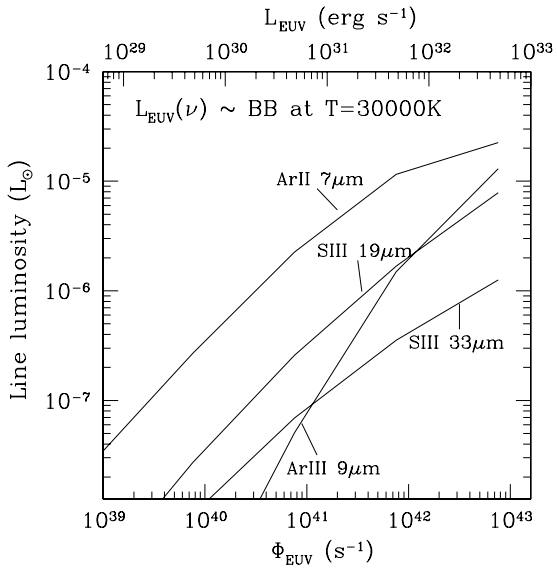

Figure 3. Dependence of [Ar II] 7 μm, [Ar III] 9 μm, [S III] 19 μm, and [S III] 33 μm line luminosities on the EUV luminosity (top in erg s^{-1} and bottom in EUV photons s^{-1}) of the central star. The EUV spectrum is assumed to be a blackbody with effective temperature $T_{\rm eff} = 30{,}000$ K. Other lines from ionized species that require >13.6 eV for their ionization are significantly weaker (see Table 1 and Equation (8)). We discuss analytic approximations for these predicted line luminosities in Section 3.1.

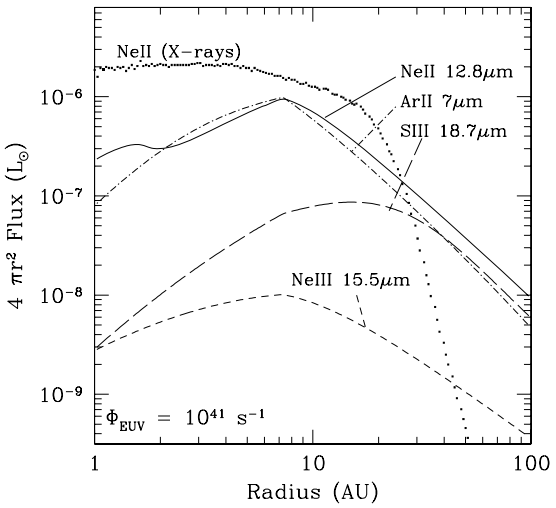

Figure 4. EUV-produced line flux emergent from one side of the disk times $4\pi r^2$ is plotted against the radius of the disk. This luminosity is approximately the luminosity emerging from both sides of an annulus between $0.5r$ and $1.5r$. The figure shows that most of the luminosity is generated at $r \sim 10$ AU. The results for a central star with $L_{\rm EUV} \simeq L_X = 2 \times 10^{30}$ erg s^{-1} are shown. In photon units, $\Phi_{\rm EUV} = 10^{41}$ s^{-1}. The EUV spectrum is assumed to be a blackbody with an effective temperature of 30,000 K (same case as Figure 2). In addition, we have plotted (dotted line) $4\pi r^2$ times the emergent flux of [Ne II] from the X-ray layer for our standard ("hard") X-ray spectrum. Substantial luminosity emerges from the region $\lesssim$1–10 AU and the overall [Ne II] luminosity is $\sim$2 times greater than the EUV layer in this case.

rapid (e.g., Butler & Dalgarno 1980), and even a neutral fraction $x(H) \sim 10^{-2}$ would lead to [Ne III]/[Ne II] < 1.

Figure 3 shows the results for a number of other fine structure transitions listed in Table 1. One sees that [Ar II] 7 μm is the strongest predicted line not yet observed. Again, the analytic estimates (Equation (8) and Table 1) are very good.

Figure 4 shows the radial origin of the EUV-induced emission in the [Ne II], [Ne III], [Ar II], and [S III] lines. We use here as a standard case $\Phi_{\rm EUV} = 10^{41}$ s^{-1} ($L_{\rm EUV} = 2 \times 10^{30}$ erg s^{-1}) and the blackbody spectrum, and $L_X = 2 \times 10^{30}$ erg s^{-1} (with our standard X-ray spectrum; see Section 4.3) although the radial origin is quite insensitive to these parameters. We see that most of the emission arises from $r \sim r_{\rm g} \sim 10$ AU, as predicted in Section 3. We plot $4\pi r^2$ times the emergent flux from one side of the disk. This roughly gives the luminosity arising from both sides of the disk and from a region extending from $0.5r$ to $1.5r$. For dominant ions such as Ne$^+$, the luminosity scales as $n_{\rm e}^2 H(r) r^2 \propto r^{1/2}$ for $r < r_{\rm g}$ and $n_{\rm e} < n_{\rm ecr}$ and as r^2 for $n_{\rm e} > n_{\rm ecr}$. The luminosity scales as $n_{\rm e}^2 r^3$ for $r > r_{\rm g}$ and $n_{\rm e} < n_{\rm ecr}$, so that here it scales as r^{-2} (see Equation (13)), as seen in [Ar II] and [Ne II]. For nondominant ions such as Ne^{++}, the scalings change because the fraction of neon in Ne^{++} changes with radius.

Hollenbach et al. (1994) and Gorti & Hollenbach (2009) showed that significant photoevaporation flows proceed in the 10^4 K gas in the EUV layer at $\gtrsim$1 AU. Thus, although our models here are static, the emitting gas is actually rising (and rapidly turning radial; see Font et al. 2004) at speeds of the order of the sound speed (or 10 km s^{-1}) from the surface of the disk. As discussed in Hollenbach et al. (1994), the electron density at the base is not much affected by this flow. Photoionization and recombination timescales are sufficiently short that the steady state still applies to the computation of the ionization state of each element in the gas. Therefore, we expect our model results on the emitted luminosities in each fine structure line to be well approximated by the static model solution. However, the observed line profiles will be affected by this flow. For a disk viewed edge-on, the lines will be broadened not only by the Keplerian rotation but also by the radial outward flow. For a disk viewed face-on, the lines will be broadened mostly by the radial outward flow, and since the far side of the disk is obscured, one would expect a blue shift. Alexander (2008b) has recently modeled [Ne II] line profiles from photoevaporating disks. He predicted broad (30–40 km s^{-1}), double-peaked profiles from edge-on disks due to rotation and a narrower ($\sim$10 km s^{-1}) profile with a significant blue shift (5–10 km s^{-1}) from face-on disks. He argued that the observed line widths in TW Hya (Herczeg et al. 2007) are consistent with a photoevaporative wind (see also Pascucci & Sterzik 2009). Resolved [Ne II] observations can thus provide a test of EUV photoevaporation models.

Figure 5 shows the vertical origin of the EUV-induced and X-ray-induced emission at $r = 10$ AU for the standard case. We have plotted gas temperature T, the dust temperature $T_{\rm dust}$, and the hydrogen nucleus density n as a function of the hydrogen nucleus column N measured from $z = r$ (the putative "surface" of the disk) downward. On the top of the figure, we give the values of z that correspond to those of N. The completely ionized EUV layer extends to $N \sim 3 \times 10^{18}$ cm^{-2} and has electron densities $n_{\rm e} \sim n \sim 3 \times 10^4$ cm^{-3} (see Equation (12)). The X-ray-heated ($T \sim 1000$ K) and ionized layer extends from $N \simeq 3 \times 10^{18}$ cm^{-2} to $N \simeq 3 \times 10^{20}$ cm^{-2} with hydrogen atom densities $\sim 3 \times 10^6$ cm^{-3}. FUV photons also contribute to the heating of this layer.

4.3. The X-ray Layer

We model the X-ray layer for both a "soft" X-ray spectrum and a "hard" X-ray spectrum. Our standard ("hard") X-ray spectrum (Gorti & Hollenbach 2004, 2008) is based on observed X-ray spectra from young stars, with an attempt to correct for extinction at the softer energies (Feigelson & Montmerle 1999). Our fit to this spectrum is that of a power law $L_\nu \propto \nu$ from

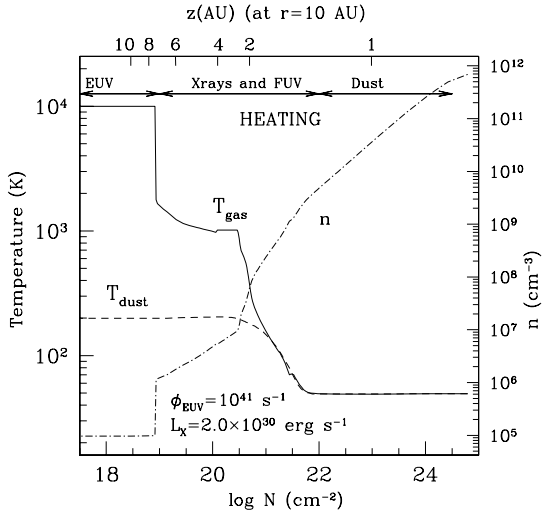

Figure 5. Gas temperature $T_{\rm gas}$, the dust temperature $T_{\rm dust}$, and the hydrogen nucleus density n are plotted versus the vertical distance z (top) from the midplane or the hydrogen nucleus column N (bottom) from the surface ($z = r$). This vertical slice is for $r = 10$ AU. The central star X-ray luminosity and EUV luminosity and spectrum are the same as in Figure 4. Note that $T_{\rm gas}$ tracks $T_{\rm dust}$ to $z \sim 2$ AU or $N \sim 10^{21}$ cm^{-2}. Higher in the disk, the gas is hotter than the dust. The EUV and X-ray layers are marked. Note that the ionization front is at $z_{\rm IF} \simeq 7.5$ AU. Dust dominates the heating of the gas near the midplane.

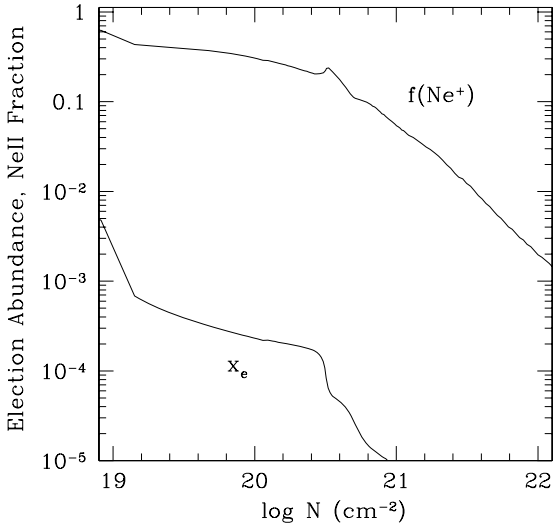

Figure 6. Fraction of neon that is in the singly ionized state, $f(\rm Ne^+)$, and the electron abundance relative to hydrogen nuclei, x_e, are plotted vs. the hydrogen nucleus column N from the disk surface at $r = 10$ AU. The EUV layer only extends to about $N \sim 10^{19}$ cm^{-2} (see Figure 5) so that we highlight here the X-ray layer. The X-ray spectrum is our harder spectrum, which peaks at ∼2 keV. X-rays maintain the high $f(\rm Ne^+)$ throughout the region plotted. X-rays maintain a relatively high electron abundance to $N \sim 10^{20}$ cm^{-2}. At higher columns, FUV photoionization of carbon as well as X-rays maintains x_e.

0.1 keV $< h\nu <$ 2 keV, fitting to another power law $L_\nu \propto \nu^{-2}$ for $h\nu >$ 2 keV. This spectrum is similar to that adopted by Glassgold et al. (2007) and Meijerink et al. (2008). We also model disks illuminated by a softer X-ray spectrum: $L_\nu \propto \nu^{-1}$ for 0.1 keV $< h\nu <$ 2 keV and $L_\nu \propto \nu^{-1.75}$ for $h\nu >$ 2 keV.[4] Ercolano et al. (2009) recently provided evidence that such a spectrum might be expected from young, low-mass stars. We note that our soft X-ray spectrum has equal energy flux in equal logarithmic intervals of photon energy between 0.1 keV and 2 keV, that is, there is as much energy flux between 0.1 and 0.2 keV as there is between 1 and 2 keV. We do not consider here a harder spectrum than our "hard" case, although recently there have been observations of "superhot" flares (Getman et al. 2008a) that indicate significant emission in the 3–8 keV region of the spectrum. We do extend our "soft" and "hard" spectra to 10 keV, but there is insignificant energy flux beyond a few keV. If there were, then for the same X-ray luminosity as our two cases, we would obtain less emission in the lines we model in this paper. The higher energy photons penetrate more column of gas, depositing less energy per unit volume, and therefore lead to cooler gas than in our current X-ray layer. In addition, because of the increased penetration, the heat is deposited in molecular regions, where the cooling is enhanced by the molecular transitions. Therefore, the emitting gas is substantially cooler and most of the X-ray heating energy presumably emerges in molecular rotation lines of, for example, CO, OH, and H_2O or possibly, if grains are abundant, as IR continuum emission from grains heated by collisions with the warmer gas. However, we emphasize that the heating and cooling timescales are long, of order 1–10 yr, so that superhot flares that are much more short-lived than this timescale will not produce a significant effect.

Glassgold et al. (2007) first modeled and discussed the physics of the X-ray layer, and our results are in basic accord with theirs, except that, as discussed below, we obtain somewhat cooler temperatures in the X-ray layer. Figure 6 shows the vertical structure of the same case plotted in Figure 5 at the same radius, $r = 10$ AU; only the N range is shrunk to emphasize the X-ray layer. In Figure 6, we plot the electron abundance x_e relative to H nuclei and the fraction of neon in Ne$^+$, $f_{\rm Ne}(\rm Ne^+)$. The [Ne II] 12.8 μm line luminosity is proportional to $x_e f_{\rm Ne}(\rm Ne^+)$ and very sensitive to T in the X-ray layer (see Figure 5 and Equation (28), where the T dependence comes in the collisional rate coefficient, which is proportional to $e^{-1100/T}$). Below the EUV layer to a depth $N \sim 3 \times 10^{20}$ cm^{-2}, X-rays maintain a relatively high fraction of Ne$^+$, $f_{\rm Ne}(\rm Ne^+) \gtrsim 10^{-2}$, and X-ray ionization of H and He as well as FUV ionization of C maintains a relatively high ionization fraction, $x_e \gtrsim 2 \times 10^{-4}$ (see Figure 6). Note that the column attenuating the X-rays in this layer is the column through the disk *to the star*, which is typically ∼10N, where N is the vertical column to the disk surface. In the X-ray layer, 10^{19} cm$^{-2} < N < 10^{21}$ cm^{-2}, the gas is heated by a combination of FUV grain photoelectric heating and X-ray photoionization heating. It is cooled mainly by [O I] 63 μm, [O I] 6300 Å, [Ne II] 12.8 μm, [Ar II] 7 μm, and gas–grain collisions (see Gorti & Hollenbach 2008). The resultant temperature is ∼1000–2000 K, dropping with increasing r and N as dilution and attenuation of the X-rays and FUV lower the heating rates. Because T, $f_{\rm Ne}(\rm Ne^+)$, and x_e drop with increasing N (see Figure 6) and r, most of the [Ne II] 12.8 μm emission arises from $r < 20$ AU and $N \sim 10^{20}$–10^{21} cm^{-2}, where $T \sim 1000$ K, $f(\rm Ne^+) \sim 10^{-1}$, and $x_e \sim 10^{-3}$.

In addition to showing the radial origin of the [Ne II] emission in the EUV layer, Figure 4 also shows the [Ne II] "luminosity" plotted as a function of r for the X-ray layer (hard spectrum X-rays). Note that there is greater contribution from inner (∼1 AU) regions of the disk compared to the EUV layer. In addition, there is more luminosity emerging from the X-ray layer than the EUV layer. Figure 4 shows that the X-ray-induced emission arises mostly from $r \sim$ 1–10 AU, also in agreement with Glassgold

[4] We note that our "soft" X-ray spectrum has the same power-law $L_\nu \propto \nu^{-1}$ form as our "hard" EUV spectrum. In addition, we note that even our "hard" X-ray spectrum includes a contribution from 0.1 keV X-rays.

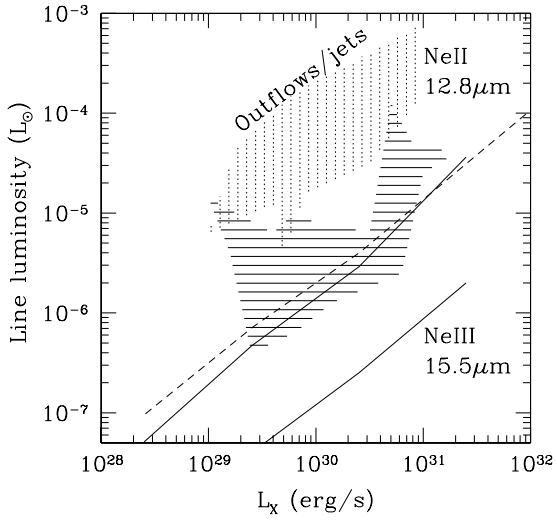

Figure 7. Dependence of [Ne II] 12.8 μm and [Ne III] 15.5 μm luminosity on the X-ray luminosity. The solid labeled lines are [Ne II] and [Ne III] for our "harder" X-ray spectrum, where $L_\nu \propto \nu$ for 0.1 keV$< h\nu <$ 2 keV. The dashed line is the [Ne II] luminosity for our softer X-ray spectrum source, where $L_\nu \propto \nu^{-1}$ for 0.1 keV $< h\nu <$ 2 keV. Note the nearly linear dependence $L_{[\mathrm{Ne\,II}]}$ on L_X. Comparison with Figure 2 shows that if $L_X \sim L_{\mathrm{EUV}}$, and assuming a soft EUV spectrum that produces the maximum amount of [Ne II], then the [Ne II] line luminosity is still 2 times stronger from the X-ray layer as from the EUV layer. A recent compilation of [Ne II] and L_X data is also plotted (Güdel et al. 2009). The region shaded with vertical dotted lines is sources with known outflows or jets. The region with horizontal solid lines is sources with undetected outflows. It appears that there are a substantial number of sources, especially the "outflow/jet" sources that are more luminous in [Ne II] than the X-ray layer (or the EUV layer) could provide; internal shocks in the winds or jets are a possible explanation for these sources.

et al. Beyond this radius, the X-ray and FUV heating is insufficient to maintain significant quantities of $T \gtrsim 1000$ K gas.

Figure 7 plots the [Ne II] 12.8 μm and [Ne III] 15 μm emissions from the X-ray layer. In agreement with Glassgold et al. (2007) and Meijerink et al. (2008) we find that [Ne III]/[Ne II] $\lesssim 0.1$, mainly caused by the rapid charge exchange of atomic H with Ne^{++}. We also plot outlines of the observed 54 sources tabulated by Güdel et al. (2009). The vertical dotted lines shade the region where the sources have known outflows and jets. The horizontal solid lines shade the regions with no outflows or jets detected. The L_X tabulated by Güdel et al. is a two-component fit with an attempt to correct for absorption of the softer X-rays by material on the line of sight from star to observer. However, many of the observations do not extend to $h\nu < 0.3$ keV and extinction is severe at the lower energies, so that a luminous soft X-ray source that is weak at 0.5–1 keV could exist undetected. The effect of such a "soft" X-ray component would be to move the data points to the right on Figure 7 and comparison should be made to our "soft" X-ray spectrum results (dashed line). We also find that $L_{\mathrm{Ne\,II}}$ and $L_{\mathrm{Ne\,III}}$ scale with L_X, as predicted in Section 3 and also as found by Meijerink et al. (2008). Comparison with Figure 2 shows that if the X-ray luminosity is about the same as the EUV luminosity from the central star, and if the EUV spectrum is soft enough that [Ne II] dominates [Ne III] in the EUV layer, the [Ne II] luminosity is roughly 2 times stronger from the X-ray layer as from the EUV layer, as we estimated analytically. The main conclusion from comparing the data to the model results is that although the X-ray layer may explain the origin of the [Ne II] emission in some (perhaps most if a strong soft X-ray excess is common) sources, there are a significant number of sources, especially those with observed outflows and jets, where the X-ray luminosity seems insufficient to explain the [Ne II] luminosity. In Section 4.4, we compare the observational data with our analytic results on the [Ne II] luminosity expected from internal shocks in the jets or winds, and find that this is a plausible origin for these sources.

As noted above, our results on the IR fine structure emission from the X-ray layer do not differ appreciably from previous results (Glassgold et al. 2007; Meijerink et al. 2008). Overall, we tend to find somewhat (factor of ~2) lower IR line luminosities. This agreement is a bit fortuitous, arising from a cancellation of several effects and the insensitivity of the fine structure lines with variations in T if $T \gtrsim 1000$ K. Our models self-consistently calculate the vertical density structure of the gas by using the computed gas temperatures (which differ from the dust temperature) to calculate the gas density structure rather than assuming that the gas density structure is fixed by the calculation of vertical pressure balance when one assumes the gas temperature to equal the dust temperature, as done in the previous work. Our self-consistent model produces significantly different results at columns $N \lesssim 10^{21}$ cm^{-2}, where the gas temperature rises above the dust temperature (Gorti & Hollenbach 2008). The net effect is that our gas disk is more flared, intercepting a larger fraction of the X-ray luminosity. This tends to raise the emission from our models. In addition, we include FUV grain photoelectric heating which also raises the emission. However, counteracting these effects is the inclusion of more gas coolants in our model, especially [Ne II] 12.8 μm and [Ar II] 7 μm. In addition, our treatment of the gas heating by X-rays follows Maloney et al. (1996), which is somewhat different than the approach used by Glassgold et al. and Meijerink et al, and our X-ray heating rates are lower than these authors by a factor of 3–10. We believe that this may arise because we include the loss of "heat" due to escape of Lyman α and other photons created by recombining hydrogen or to the absorption of these photons by dust. Overall, our X-ray layer tends to be a factor of about 2 cooler than the previous models (roughly 1000–2000 K versus 2000–4000 K in the previous models), thereby lowering the fine structure emission from this layer. This lower temperature has a relatively small effect on the fine structure lines, because their upper states lie only $\Delta E/k \sim 1000$ K above the ground state. However, it has an enormous effect on our predictions of the [O I] 6300 Å emission, whose upper state lies $\Delta E/k \sim 23{,}000$ K above the ground state, as we will discuss in Section 4.5.

4.4. [Ne II] Emission from Internal Shocks in the Jets and Winds

Figure 8 plots the [Ne II] luminosity versus the mass accretion rates assembled by Güdel et al. (2009). As in Figure 7, the vertical dotted lines shade the region that includes sources with known jets or outflows, whereas the solid horizontal lines denote sources with no detected jets/outflows. We plot here our predicted [Ne II] luminosities from internal shocks in the winds/jets, using our analytic expression (Equation (33)). The solid line represents the expected [Ne II] luminosity when $\dot{M}_{\mathrm{w}} = 0.1\dot{M}_{\mathrm{acc}}$, the entire wind or jet passes through a shock or $f_{\mathrm{sh}} = 1$, the shock velocity is in excess of about 100 km s^{-1}, and the preshock density is less than 10^4 cm^{-3}. The upper dashed line makes the same assumptions except that $\dot{M}_{\mathrm{w}} = \dot{M}_{\mathrm{acc}}$ and the lower dashed line assumes $\dot{M}_{\mathrm{w}} = 0.01\dot{M}_{\mathrm{acc}}$. Note that the [Ne II] luminosity is proportional to the product of f_{sh} and $\dot{M}_{\mathrm{w}}$, so that, for example, the lower dashed line also corresponds to $f_{\mathrm{sh}} = 0.1$ and $\dot{M}_{\mathrm{w}} = 0.1\dot{M}_{\mathrm{acc}}$. The main conclusion is that internal wind

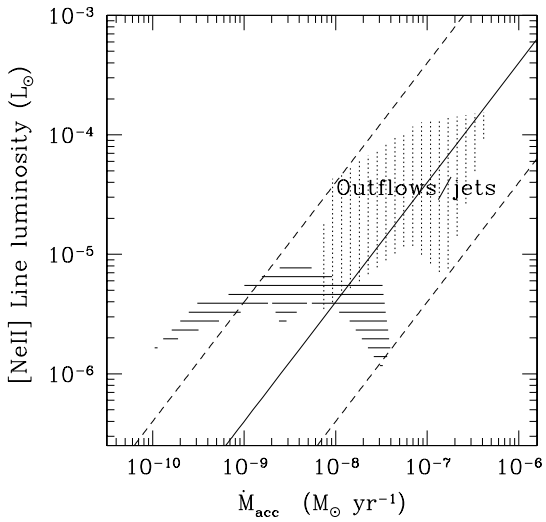

Figure 8. Dependence of the [Ne II] 12.8 μm luminosity on the mass accretion rate onto the central star. The shaded regions are of the same notation as in Figure 7; data from Güdel et al. (2009). Section 3.4 in the text and Equation (33) predict the [Ne II] luminosity as a function of the wind or jet mass loss rate $\dot{M}_{\rm w}$ and the fraction $f_{\rm sh}$ of the wind or jet that shocks at speeds greater than about 100 km s^{-1}. The solid line in the figure assumes $\dot{M}_{\rm w} = 0.1\dot{M}_{\rm acc}$ and $f_{\rm sh} = 1$. The upper dashed line assumes $\dot{M}_{\rm w} = \dot{M}_{\rm acc}$ and $f_{\rm sh} = 1$. The lower dashed line assumes that the product $f_{\rm sh}\dot{M}_{\rm w}$ is 10 times less than assumed in the solid line case. Shocks appear as viable explanations for the origin of many of the [Ne II] sources, especially those with observed outflows and jets (see also Figure 7).

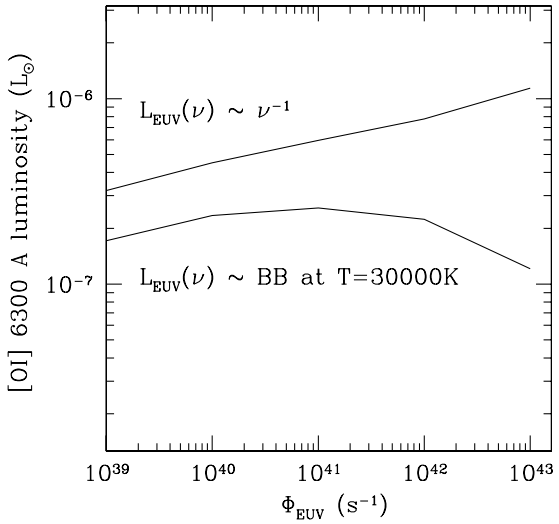

Figure 9. Predicted [O I] 6300 Å luminosity from the EUV layer is plotted for both a blackbody EUV spectrum ($T_{\rm eff} = 30{,}000$ K) and a power-law spectrum as a function of the EUV photon luminosity $\Phi_{\rm EUV}$. The harder spectrum produces more [O I] luminosity because more atomic O survives in the mostly ionized EUV layer (see text). Observed [O I] luminosities are typically much higher than $\lesssim 10^{-6}\,L_\odot$ predicted from the EUV layer (see text).

or jet shocks very likely explain the origin of [Ne II] from the outflow and jet sources. In fact, the figure might suggest that these shocks could explain [Ne II] observed in nearly all of the sources, if it were not for the fact that in some cases (e.g., Herczeg et al. 2007; Najita et al. 2009; Pascucci & Sterzik 2009) where the lines have been spectrally resolved, they are narrower than what a shock origin would predict. We do note that in some of these cases, the integrated flux seen with the high spectral and spatial resolution ground-based instruments is significantly less than the flux seen by the low resolution *Spitzer Space Telescope*. Najita et al. speculated that perhaps there are two components comprising the total flux: a strong but broad and extended shock component and a weaker, but narrow and spatially unresolved disk component arising from the X-ray layer. On the other hand, it is quite possible that X-rays or EUV produce most of the [Ne II] luminosity in the sources with no observed winds or jets. Note that these sources in Figure 8 are distributed in a nearly horizontal line with no apparent dependence on $\dot{M}_{\rm acc}$ over a two orders of magnitude increase in this parameter.

4.5. [O I] 6300 Å Emission from the Extreme Ultraviolet and X-Ray Layer

Figure 9 plots the [O I] 6300 Å luminosity from the EUV layer versus $\Phi_{\rm EUV}$ for both our harder $L_{\rm EUV}(\nu) \propto \nu^{-1}$ spectrum and our softer $L_{\rm EUV}(\nu)$ blackbody spectrum. A harder spectrum gives more [O I] luminosity in the EUV layer because although the gas is almost entirely ionized, there is a greater fraction of neutral H and O in the gas due to the smaller photoionization cross section of these atoms with higher photon frequency. However, even the harder EUV spectrum results in [O I] 6300 Å luminosities $\lesssim 10^{-6}\,L_\odot$, which can only explain the weakest LVC sources. Recall that $L_{\rm [O\,I]}$ ranges from 10^{-6} to $10^{-3}\,L_\odot$ in LVCs.

Figure 10 plots the [O I] 6300 Å luminosity in the X-ray layer versus L_X for both our harder and our softer X-ray spectra.

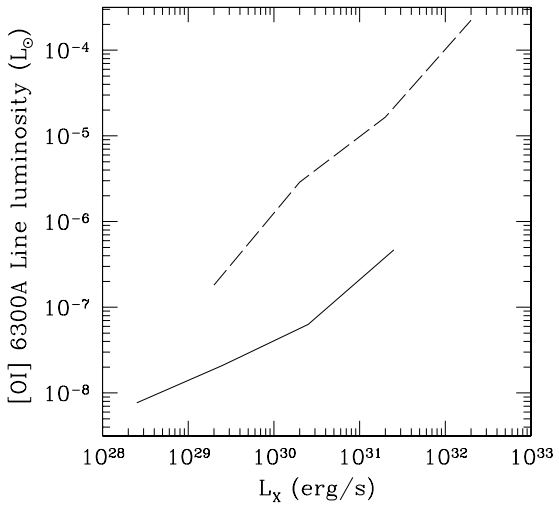

Figure 10. Predicted [O I] 6300 Å luminosity from the X-ray layer is plotted versus the X-ray luminosity of the central star. The solid line is for our harder X-ray spectrum whereas the dashed line is for our softer X-ray spectrum (see text or caption to Figure 7). Observed [O I] luminosities are typically much higher than the $\lesssim 10^{-6}\,L_\odot$ predicted from the X-ray layer produced by the harder spectrum. However, the softer X-ray spectrum produces [O I] luminosities much more in accord with observations, because the X-ray layer is warmer and the line is extremely temperature sensitive (see text).

The [O I] luminosity does increase with L_X, due to the higher temperatures and higher ionization fractions in the X-ray layer. Recall that the gas is primarily neutral, so the higher ionization fraction increases the luminosity by increasing the density of the electrons that excite [O I]. However, with our standard (harder) X-ray spectrum, which is quite similar to that adopted by Meijerink et al. (2008), we obtain [O I] luminosities that are a factor of nearly 100 times lower than those of Meijerink et al. (2008) from the X-ray layer. This is primarily because of the extreme sensitivity of the [O I] luminosity to the temperature of the X-ray layer (see Equation 38). As noted above, our temperatures are roughly a factor of 2 lower than those of Meijerink et al.

The main point, however, is that in our standard models neither the EUV layer nor the X-ray layer can produce [O I] luminosities as high as 10^{-5}–10^{-3} $L_\odot$ as observed in many LVC sources. This confirms the analytic estimates made in Section 3.5. However, as discussed above, the [O I] luminosity is very sensitive to the temperature of the X-ray layer. One way to increase the temperature is to assume a softer X-ray spectrum. Softer X-rays have much higher absorption cross sections and therefore deposit much more heat per unit volume in the upper layers. In addition, they create higher electron abundances, and these lead to increased efficiency in converting the absorbed X-ray energy into heat. Therefore, we also plot in Figure 10 the results for cases with similar X-ray luminosities, but with our "soft" X-ray spectrum where $L_\nu \propto \nu^{-1}$ from 0.1 keV to 2 keV. This spectrum has many more 0.1–0.3 keV X-rays than our standard case, and we find that we do indeed get higher temperatures and electron abundances in the upper parts of the X-ray layer and consequently much higher [O I] luminosities. $L_{[O\,I]}$ can be as high as $\sim 10^{-4} L_\odot$ if $L_X \sim 10^{32}$ erg s^{-1} ($\sim 2\times10^{-2}$ $L_\odot$), a likely upper limit to the soft X-ray luminosity. Therefore, soft X-rays may be able to explain "typical," $L_{[O\,I]} \sim 10^{-4}$ $L_\odot$, LVC sources, but not the most luminous sources. We note that if the soft X-rays caused photoevaporation, then high spectral resolution observations of the [O I] line might diagnose the flow parameters.

5. DISCUSSION

This paper has focused on fine structure lines from ions that required $h\nu > 13.6$ eV photons to photoionize them. Most of these lines fall in the 5 μm $< \lambda <$ 40 μm wavelength region and are therefore partially accessible through atmospheric windows from the ground and entirely accessible from space-based observatories such as the *Spitzer Space Telescope*. Ground-based observatories have the advantage of larger diameter telescopes and therefore greater spatial resolution as well as larger and heavier instruments capable of higher spectral resolution. The TEXES instrument (Lacy et al. 2002) achieves a spectral resolution of $\sim$3 km s^{-1} and a spatial resolution of $\sim 0.5(\lambda/10\ \mu\mathrm{m})$ arcsec on a 10 m class ground-based telescope such as Gemini. Its sensitivity to line flux (5σ in 1 hr) translates to $L \sim 3\times10^{-7}$ $L_\odot$ at 100 pc. The Michelle instrument (Glasse et al. 1997) achieves a spectral resolution of $\sim$15 km s^{-1} and is capable of detecting lines with luminosities $L \sim 3\times10^{-6}$ $L_\odot$ at 100 pc, if mounted on a 10 m class ground-based telescope. The VISIR instrument on an 8 m class telescope has a sensitivity of $\sim 3\times10^{-6}$ $L_\odot$ at 100 pc and a spectral resolution of about 12 km s^{-1} (Lagage et al. 2004). *Spitzer* had relatively poor spatial ($\sim$12 arcsec resolution) and spectral ($\sim$500 km s^{-1}) resolution but could achieve 5σ in 1 hr sensitivity that translated to $L \sim 10^{-7}$ $L_\odot$ at 100 pc.

A number of groups have now observed nearby star-disk systems and measured fluxes from especially the [Ne II] 12.8 μm line, with a few detections of H I recombination lines and good upper limits for [Ne III] 15 μm lines. Many of the observations were done using the IRS spectrometer on *Spitzer* (Espaillat et al. 2007; Lahuis et al. 2007; Pascucci et al. 2007; Ratzka et al. 2007).

However, we first discuss recent ground-based observations with high resolution spectroscopy that help constrain the origin of the Ne II emission by interpretation of the observed linewidths and spatial extents, as well as by the observed fluxes (e.g., Herczeg et al. 2007; van Boekel et el. 2009; Najita et al. 2009; Pascucci & Sterzik 2009). The first such resolved source to be observed and also one of the brightest is TW Hya (Herczeg et al. 2007). Herczeg et al. interpreted the observed line width ($\sim$21 km s^{-1}) from this nearly face-on disk as possibly indicating that the emission arises from the inner regions ($\sim$0.1 AU) of the disk. In our models, it is very difficult to produce the observed [Ne II] luminosity from X-rays or EUV at 0.1 AU. However, as they noted, it might also originate from the EUV or X-ray layers at $r \sim 10$ AU, if turbulence can produce the observed linewidths. Alternatively, the linewidth may arise from the fact that the gas is not merely in Keplerian rotation but is also photoevaporating at $\sim$10 km s^{-1} with respect to the disk surface. This produces a blue shift of [Ne II] with respect to the stellar velocity (e.g., Alexander 2008b). Using the VISIR spectrograph on the Very Large Telescope (VLT) *Melipan*, Pascucci & Sterzik (2009) recently showed that nearly all the line flux is blueshifted, with a peak at -6.3 km s^{-1} and a FWHM of 14.2 km s^{-1}. They pointed out that these observations are in near perfect agreement with the prediction of Alexander (2008b) for [Ne II] produced in an EUV-induced photoevaporating flow and inconsistent with a static disk atmosphere. Alternatively, a soft X-ray spectrum might produce a very similar photoevaporating profile, since soft X-rays heat the disk surface at 1–10 AU to almost the same temperatures as the EUV layer. We note that TW Hya is known to have a strong soft X-ray excess (Kastner et al. 2002). The measured low accretion rate, 5×10^{-10} $M_\odot$ yr^{-1} (Muzerolle et al. 2000), and the absence of any known outflow support an EUV and/or X-ray-heated disk origin for the [Ne II] emission. The observed [Ne II] luminosity as measured by Pascucci & Sterzik is $\sim 4\times10^{-6}$ $L_\odot$. From our models, we predict no contribution from shocks that is consistent with the low observed linewidths. We would expect EUV and X-rays to irradiate the disk given the low accretion rate and the measured flux to be a sum of the contributions from the ionized and neutral layers of the disk. We calculate the contribution from the neutral layer to be $\sim 3\times10^{-6}$ $L_\odot$ (using $L_X = 2\times10^{30}$ erg s^{-1}; Kastner et al. 2002). If the remaining $\sim 10^{-6}$ $L_\odot$ is from the ionized layer, we then estimate that $\Phi_{\mathrm{EUV}} = 3\times10^{40}$ s^{-1} for TW Hya. However, given the accuracy of our models, we cannot rule out that most of the [Ne II] emission is from the EUV layer ($\Phi_{\mathrm{EUV}} = 1.2\times10^{41}$ s^{-1}). The excellent agreement of the [Ne II] line profile with the EUV model suggests that EUV may dominate in this source, but our model results using the observed X-ray luminosity suggest that a substantial amount of [Ne II] may arise in the X-ray layer. Modeling of X-ray-induced flows and further observations are needed to clarify this discrepancy, possibly of the [Ar II] 7 μm line which might discriminate between the [Ne II] emission from EUV or X-ray layers (see the discussion below at the end of this section).

Herczeg et al. failed to detect [Ne II] emission for the sources BP Tau and DP Tau. These nondetections are also compatible with the [Ne II] emission models described in this paper. BP Tau is an actively accreting star ($\sim 2\times10^{-8}$ $M_\odot$ yr^{-1}; Muzerolle et al. 2000) with presumably no EUV penetration of the disk wind and an X-ray luminosity ($L_X \sim 7\times10^{29}$ erg s^{-1}) that would produce lower [Ne II] emission than the upper limit from observations. DP Tau has a low accretion rate, but very poor upper limits to the [Ne II] flux to provide any reasonable estimates of Φ_{EUV}.

Van Boekel et al. (2009) reported that the [Ne II] emission from the T Tau triplet, which is resolved spatially and spectrally, has large linewidths $\sim$100 km s^{-1} and is associated with a known outflow. Even though T Tau N is a very strong X-ray source with $L_X \sim 2\times10^{31}$ erg s^{-1} (Güdel et al. 2007), the expected [Ne II] from the disk is still a factor of $\sim$10 lower

than what is observed. In addition, van Boekel et al. spatially resolved the [Ne II] emission and determined that it arises from T Tau S. We do not expect EUV and soft X-rays to penetrate the disk wind for this young source. On the other hand, our models of shock emission are consistent with the van Boekel et al. data, as discussed in Section 3.4. van Boekel et al. also concluded that shock emission is the likely origin of the [Ne II] emission.

Najita et al. (2009) have observed two young disks around AA Tau and GM Aur using TEXES on Gemini N and spectrally resolved the [Ne II] line in both the sources. The FWHM linewidths are 70 and 14 km s^{-1}, respectively, and the authors interpreted the emission as arising from the X-ray layer in Keplerian disks. They also noted that the flux in the line is less than that measured by the much larger beam of *Spitzer*. A spatially extended and broad (FWHM) additional component, such as a protostellar wind shock, could account for the difference. GM Aur is a transition disk object, which is still actively accreting at $\sim 10^{-8}\,M_\odot$ yr^{-1}, indicating the presence of gas in the dust depleted inner disk. The disk accretion rate is at a marginal epoch where the EUV may make it through to irradiate the disk or may be absorbed by the disk wind. From the known X-ray luminosity of the star ($L_X \sim 10^{30}$ erg s^{-1}; Strom et al. 1990), we estimate an X-ray-produced [Ne II] line luminosity of $2 \times 10^{-6}\,L_\odot$, while the observed value is $\sim 7 \times 10^{-6}\,L_\odot$ (Najita et al. 2009). The rest may arise from shocks, although no known outflows exist. Alternately, it may come from either an unobserved EUV or a soft X-ray component that has just begun to penetrate the disk wind and heat and ionize the surface layers. Note that if EUV dominates, $\Phi_{\rm EUV} \sim 2 \times 10^{41}$ s^{-1}. The classical T Tauri star, AA Tau, has a low accretion rate for an object of its class, estimated at $3 \times 10^{-9} M_\odot$ yr^{-1} (Gullbring et al. 1998), and we expect irradiation of the disk by EUV and X-ray photons due to the expected low wind column density. The observed line luminosity is $\sim 4 \times 10^{-6}\,L_\odot$. AA Tau is highly X-ray variable with $L_X \sim 3 \times 10^{30}$–$2 \times 10^{31}$ erg s^{-1} (Schmitt & Robrade 2007), which can result in Ne II luminosities arising from the X-ray-heated neutral layer, ranging from $10^{-6}\,L_\odot$ to $10^{-5}\,L_\odot$, and the observed value lies within this range. While it is likely that the X-ray layer explains the origin of [Ne II], the observed [Ne II] flux places an upper limit of $\Phi_{\rm EUV} \lesssim 2 \times 10^{41}$ s^{-1} for AA Tau.

Pascucci & Sterzik (2009) detected [Ne II] in all the three transition disks that they observed (TW Hya, CS Cha, T Cha), but only from one of the three classical disks (Sz 73). They claimed that the resolved linewidths of all the transition disks are consistent with a photoevaporative flow driven by stellar EUV photons and estimated $\Phi_{\rm EUV} \sim 10^{41-42}$ s^{-1}. These numbers should be considered as upper limits to $\Phi_{\rm EUV}$ since there may be some contribution to the [Ne II] flux from the X-ray layer. Pascucci & Sterzik also observed blueshifted [Ne II] emission in CS Cha and T Cha, consistent with EUV photoevaporation. In CS Cha, the inferred hole size is 45 AU. We note that if the inner disk is completely clear of gas, such a large hole is only consistent with EUV-induced [Ne II] emission since the X-ray flux at this radius is too low to heat the gas to temperatures $\gtrsim$1000 K required to excite [Ne II]. Pascucci & Sterzik pointed out that they only detected such evidence of EUV photoevaporation in sources with very low accretion rates, consistent with our model here that EUV does not penetrate the wind base until the accretion rates are low. We also note that the expected X-ray-heated [Ne II] emissions for their nondetections are consistent with their upper limits.

We next discuss the totality of [Ne II] observations, which is dominated by unresolved *Spitzer* sources. There is clearly a considerable amount of scatter when one tries to see if the [Ne II] luminosities $L_{\rm Ne\,II}$ correlate with either the X-ray luminosity L_X or with $\dot{M}_{\rm acc}$. Espaillat et al. (2007) concluded that [Ne II] has a nearly linear correlation with the mass accretion rate; they found a 10 times increase in [Ne II] luminosity with about a 10-fold increase in the accretion rate.[5] However, Espaillat et al. had a data set of only seven sources, whereas recently Güdel et al. (2009) have compiled a data set of more than 50. Güdel et al. found little $L_{\rm Ne\,II}$ dependence on mass accretion rates at low $\dot{M}_{\rm acc} \lesssim 3 \times 10^{-8}\,M_\odot$ yr^{-1}, but a roughly linear trend in the high $\dot{M}_{\rm acc} \gtrsim 3 \times 10^{-8}\,M_\odot$ yr^{-1}, sources which show evidence for jets and outflows (see Figures 7 and 8). The latter suggests that protostellar wind shocks may be responsible for [Ne II] from the outflow sources. It seems unlikely that [Ne II] in these sources is due to soft X-rays or EUV, since the wind mass loss rates are sufficiently high to likely block these photons from ever striking the disk surface at radii near $r_{\rm g}$. In addition, our analytic predictions of [Ne II] luminosities from wind shocks seem to match the observations (Figure 8). Espaillat et al. found little correlation of $L_{\rm Ne\,II}$ with L_X. Güdel et al. formally found $L_{\rm Ne\,II} \propto L_X^{0.58}$ but with a tremendous amount of scatter. We note that although many of the observed X-ray luminosities derive from observations of ~0.2–10 keV X-rays, the soft (0.1–0.3 keV) X-rays may suffer considerable extinction that is difficult to estimate, and considerable luminosity could be "hidden" in such a soft component. Some of the observed scatter may then be caused by [Ne II] arising from EUV, soft X-ray, or shock-heated and ionized gas.

In summary, shocks may dominate at high $\dot{M}_{\rm acc} \gtrsim 3 \times 10^{-8}\,M_\odot$ yr^{-1}, but there is observational evidence that EUV or X-rays must dominate at lower accretion rates. Because X-rays are more efficient in producing [Ne II], in naturally producing [Ne II] stronger than [Ne III] as observed, and in more easily penetrating the base of the protostellar wind, it seems likely that X-rays often dominate the EUV production of [Ne II] in disks, although not by a large factor. A part of this evidence for a nonshock origin has been gathered by high spectral resolution observations of [Ne II] made by ground-based telescopes, which show relatively small linewidths compared to the $\gtrsim$100 km s^{-1} linewidths expected for wind-shocked [Ne II]. Although ~1 keV X-rays may play a role in the production of $L_{\rm Ne\,II}$ for sources with weak winds, there is clear evidence that EUV or soft X-rays may sometime dominate. If one wanted to identify a source where it is likely that either EUV or soft X-rays dominate the [Ne II] production, one would choose sources with low accretion rates, $\dot{M}_{\rm acc} \lesssim 8 \times 10^{-9}\,M_\odot$ yr^{-1}, whose $L_{\rm Ne\,II}$ lies well above the observed correlation of $L_{\rm Ne\,II}$ with the 1 keV L_X.

One of our principal results is that X-rays are more efficient in producing [Ne II] emission than are EUV photons. If the central star has the same luminosity in X-rays as it does in EUV photons, the [Ne II] luminosity from the X-ray layer will be about 2 times greater than [Ne II] from the EUV layer (assuming a soft EUV spectrum, which is most efficient in producing [Ne II]). This result was shown both analytically, in Section 3, and in our numerical results, as seen in Figures 2 and 7. Since the [Ne II] luminosity scales linearly with the EUV luminosity and with the X-ray luminosity, this means that the EUV luminosity needs to be at least 2 times the X-ray luminosity for the EUV to

[5] We note that Pascucci et al. (2007) found a tentative anticorrelation with accretion rate, but this was based on a very limited data set which had a small range in values of line luminosity and accretion rates.

dominate the production of [Ne II]. Unfortunately, we have little idea of the EUV luminosity, since it is impossible to observe in young sources. Observations of older, nearby stars by Ribas et al. (2005) suggested that the luminosity in the EUV band is usually similar to that of the X-ray band. However, these sources are not accreting, and it is possible for an accreting source to be very bright in EUV relative to 1 keV X-rays (but see Alexander et al. 2004b; Glassgold et al. 2009, who argued these photons are attenuated by the accretion columns near the star). In any event, these accreting stars need to have sufficiently low wind mass loss rates to allow these accretion shock-generated EUV photons to penetrate the wind base and strike the outer disk to create EUV-generated [Ne II]. Alexander et al. (2005) estimated EUV fluxes from stars with observed ultraviolet emission lines and concluded that in some cases, the EUV photon luminosities can be as high as 10^{44} s^{-1}. This suggests that in some cases, the chromospheric emission may generate more EUV luminosity than X-ray luminosity in young stars. However, our own results place upper limits on the possible EUV photon luminosities: $\Phi_{\rm EUV} \lesssim 10^{42}$ s^{-1}. Overall, it appears that it is unlikely that the EUV fluxes on the disk surface are any stronger than the X-ray fluxes and that it is likely that X-rays often slightly dominate EUV photons in the production of [Ne II] when the wind mass loss rates are low so that internal wind shocks are weak.

We have plotted the observed [Ne II] and [Ne III] data in Figure 7, using the compilation of Güdel et al. (2009) that uniformly treats all previously observed sources. The observed [Ne III]/[Ne II] ratio of less than 0.06 in the source with measurements of both lines (Sz102, Lahuis et al. 2007) favors either an origin in the X-ray layer, a shock, or in a soft ($T_{\rm eff} \lesssim 40{,}000$ K) EUV layer. A hard EUV layer such as our adopted power law $F_\nu \propto \nu^{-1}$ is ruled out. Several of the sources have [Ne II] luminosities readily explained as arising in the X-ray regions, as noted by Meijerink et al. (2008). However, a number of the sources have larger [Ne II] luminosities than can be explained by $\gtrsim$0.5 keV X-rays alone. In many such cases, such as the T Tau South source discussed by van Boekel et al. (2009), shocks in the protostellar wind are the likely source. We note that since wind mass loss rates scale with accretion rates, shocks would provide the observed correlation (Espaillat et al. 2007; Güdel et al. 2009) between the mass accretion rate and $L_{\rm [Ne\,II]}$ (see Figure 8).

If the wind mass loss rates are not sufficient to provide the observed [Ne II] luminosity, or if ground-based observations reveal narrower lines than might be expected from the shocks, such as in TW Hya, [Ne II] emission may be generated by a soft EUV or X-ray spectrum from the central star. Since the "hard" X-rays were insufficient to explain some of these sources, and since we have shown that X-rays are more efficient in producing the [Ne II] line, the only way that EUV luminosity from the central star can explain these sources is for the EUV luminosity to be greater (>2 times) than the observed X-ray luminosity and, in addition, the EUV spectrum has to be "soft" ($T_{\rm eff} \lesssim 40{,}000$ K). If EUV does dominate, we can see from Figures 1 and 7 that $L_{\rm EUV} \lesssim 10^{-2}\,L_\odot$ is often required. A luminosity of $10^{-2}\,L_\odot$ corresponds to $\Phi_{\rm EUV} \sim 10^{42}$ s^{-1}. The comparison of the [Ne II] and [Ne III] data with Figures 1 and 2 gives hard upper limits on $\Phi_{\rm EUV}$. Most sources have $\Phi_{\rm EUV} \lesssim 10^{42}$ s^{-1}. If EUV is the main excitation mechanism, the comparison actually measures $\Phi_{\rm EUV}$ and the [Ne II]/[Ne III] ratio constrains the EUV spectrum.

We have examined our model results for diagnostics that would reveal whether the [Ne II] emission arises from the EUV layer or from the X-ray layer. One possible diagnostic is the ratio of the [Ne II] 12.8 μm line to the [Ar II] 7 μm line, [Ne II]/[Ar II]. We have shown in Figures 2 and 3, along with the analytic calculation Equation (8)) combined with Table 1, that in the EUV layer the [Ne II]/[Ar II] ratio is about unity for our "soft" EUV spectrum. This spectrum maintains most Ne and Ar in a singly ionized form in the EUV layer. Although elemental Ar is 20 times less abundant in the H II gas than Ne, the rate coefficient for electronic excitation of the [Ar II] line is about 10 times larger than that of [Ne II], and the 7 μm line has almost twice the photon energy as the 12.8 μm line, making up for the abundance discrepancy. In the X-ray layer, most of the Ne and Ar is neutral, and the fractional abundance of Ne^+ and Ar^+ depends, in addition to elemental abundances, on the X-ray photoionization cross sections of Ar and Ne, on the electron rate coefficients for collisional ionization of Ar and Ne by secondary electrons, and on the rate coefficients for electronic recombination of Ne^+ and Ar^+. In addition, the [Ar II] line lies $\Delta E/k \simeq 2060$ K above ground, whereas the [Ne II] line lies only $\simeq$ 1100 K above ground. Since the X-ray-heated gas is typically $\sim$1000 K, this means that the relative line strengths are sensitive to the temperature of the X-ray-heated layer, with [Ar II] gaining advantage in warmer gas relative to [Ne II]. We find in our models that for our hard X-ray spectrum, which peaks at 2 keV and where Ne and Ar are ionized mainly by direct X-ray photoionization, the X-ray layer produces [Ne II]/[Ar II] $\simeq$ 2.5. Unfortunately, due to a coincidence of atomic parameters and the enhanced heating due to soft X-rays, for our soft X-ray spectrum the ratio is [Ne II]/[Ar II] $\simeq$ 1, *the same as in the EUV layer*. Thus, this ratio may discriminate between [Ne II] produced in the X-ray layer and the EUV layer only when the X-ray spectrum is relatively "hard." Nevertheless, a large ratio would strongly point to an origin in the X-ray layer.

We have also examined both analytically and numerically the expected [O I] 6300 Å luminosity from disks around young stars. The observed luminosities in this line range from 10^{-6} to $10^{-3}\,L_\odot$ in the LVC, which has been identified as arising from the disk. We have shown that the EUV, transition, and (hard) X-ray layers are not likely to produce [O I] 6300 Å luminosities greater than $10^{-6}\,L_\odot$. Meijerink et al. (2008) provided models utilizing a relatively "hard" X-ray spectrum (peaking around 1 keV), which achieved [O I] luminosities as high as $\sim 10^{-4}\,L_\odot$, but our models with a similar X-ray spectrum give [O I] luminosities $\sim 10^{-6}\,L_\odot$. The [O I] 6300 Å line is extremely sensitive to the temperature in the X-ray layer, as we showed analytically in Section 3.5. Our models give typical temperatures of 1000–2000 K, whereas the Meijerink et al. models give 2000–4000 K. We discussed in Section 4.3 the improvements in our models that lead to lower gas temperatures in the X-ray layer. However, Ercolano et al. (2009) appealed to observational constraints on the emission measure distribution as a function of temperature for the chromospheres of young star analogs to argue that there is a (largely unobserved) soft X-ray component that is much larger than that assumed in our standard X-ray spectrum and in Meijerink et al. (2008). Ercolano et al. found that the X-ray spectrum may be better approximated by a power law $L_\nu \propto \nu^{-1}$ from 0.1 keV to 2 keV. We have also run cases with such a soft X-ray spectrum and found that X-ray luminosities of $\sim 10^{32}$ erg s^{-1} can then give rise to [O I] luminosities of $\sim 10^{-4}\,L_\odot$.

6. SUMMARY AND CONCLUSIONS

Circumstellar disks around low-mass stars evolve with time with a decreasing accretion rate onto the star and a decreasing wind mass loss rate from the inner disk. X-rays, EUV, and FUV photons from young, low-mass stars arise principally from either magnetic activity (an active chromosphere) or from the accretion shock arising as disk material falls onto the star, presumably in accretion columns along stellar magnetic field lines. In the latter case, the energetic photons must penetrate or obliquely avoid the accretion columns in order to illuminate the disk surface. In either case, they must penetrate the protostellar wind near the wind base. We treat here the penetration of the protostellar wind and find that FUV photons likely penetrate first, when the wind mass loss rate is $\dot{M}_{\rm w} \gtrsim 4 \times 10^{-8}\,M_\odot$ yr^{-1}, the exact number depending on the very uncertain dust opacity in the wind base material. As the wind mass loss rate drops with time, ~1 keV X-rays penetrate next, when $\dot{M}_{\rm w} \simeq 4 \times 10^{-8}\,M_\odot$ yr^{-1}. Finally, soft (~0.1 keV) X-rays and EUV photons penetrate only when the wind can be fully ionized at the base, which occurs roughly at $\dot{M}_{\rm w} \lesssim 8 \times 10^{-10}\,M_\odot$ yr^{-1}. The corresponding mass accretion rates onto the star are about 10 times higher, with considerable scatter. Considering the observed rates of mass accretion with time (e.g., Hartmann et al. 1998), these criteria translate to FUV and 1 keV X-rays penetrating very quickly after mass infall onto the disk from the molecular core has ceased, whereas EUV and soft X-rays may require an additional 1–2 Myr (with a lot of scatter) before they illuminate the disk.

The 1 keV X-rays and FUV photons penetrate the disk surface to vertical columns of $N \sim 10^{21}$ cm^{-2} and heat this layer to temperatures of order 1000 K for $r \lesssim$ 10–20 AU. The X-rays ionize hydrogen and atoms with IPs >13.6 eV in this predominantly neutral layer, providing both electrons and species such as Ne^+ and Ar^+. Thermal collisions of the electrons with these species produce fine structure lines such as [Ne II] 12.8 μm. The high gas temperatures and elevated electron abundances also produce strong emission from the [O I] 6300 Å forbidden line in regions with $T \gtrsim 2000$ K. The FUV photodissociates molecules, ionizes species with IP < 13.6 eV, and contributes to the gas heating.

The EUV photons incident upon the disk create a fully ionized (H II) layer with $T \sim 10^4$ K, which lies above the X-ray layer on the disk surface. Here, EUV photoionizes species with IP $\gtrsim$13.6 eV and singly or doubly ionized species tend to be the dominant ionization stage. Trace amounts of atomic oxygen are present and a relatively small amount of [O I] 6300 Å luminosity emerges from this layer. Due to a combination of falling electron density, rising scale height, and increasing disk surface area with increasing r, most of the fine structure emission from the EUV layer arises from $r \sim r_{\rm g} \sim 7(M_*/1\,M_\odot)$ AU. The EUV layer produces more hydrogen recombination line luminosity than the X-ray layer, but does not explain the observed high ratio of these lines to [Ne II]. It is likely that the hydrogen recombination lines are produced in dense plasma close to the star: in the chromosphere, the accretion shock, or in a wind shock very close to the star.

Strong ($\gtrsim$100 km s^{-1}) shocks, such as can be produced in internal shocks in protostellar winds or jets, can also significantly ionize species with IP >13.6 eV and heat the gas to $T \gg 1000$ K, sufficient to excite the fine structure lines, the hydrogen recombination lines, and optical forbidden lines such as [O I] 6300 Å. Such ionization and heating have been inferred by the observation of optical lines emitted in knots in the jets and in Herbig–Haro objects.

In this paper, we have analytically modeled all three of these emitting regions and have presented results from detailed thermo/chemical numerical models of the EUV and X-ray layer. We have focused on the emergent line luminosities of [Ne II] 12.8 μm, [Ne III] 15.5 μm, [Ar II] 7 μm, [Ar III] 9 μm, [S III] 19 μm, [S III] 33 μm, and [O I] 6300 Å. However, we also discussed IR hydrogen recombination lines (6–5 and 7–6) and other fine structure lines such as [S IV], [N II], [N III], and [O III]. These line luminosities are diagnostic of key parameters such as the EUV luminosity and spectral shape, the X-ray luminosity and spectral shape, and the wind mass loss rate and shock speed. Our main results are as follows.

1. The luminosity of fine structure lines (e.g., [Ne II] and [Ar II]) from the dominant ionization state of a species roughly scale with L_X and $L_{\rm EUV}$. At very high L_X or $L_{\rm EUV}$, the lines saturate because the electron density in the emitting region exceeds the critical density of the line. [Ar II] 7.0 μm, which has not yet been observed, is predicted to be as strong as [Ne II] 12.8 μm in the EUV layer. If the X-ray layer dominates and the X-ray spectrum is such that much of the X-ray luminosity is in the 1–3 keV band, the [Ar II] line is predicted to be about 2.5 times weaker than the [Ne II] line. Therefore, the observed [Ne II]/[Ar II] flux ratio may help determine the origin of these lines. Observations of [Ne II] set upper limits for the EUV luminosity of the central star, $\Phi_{\rm EUV} \lesssim 10^{42}$ EUV photons s^{-1} for most sources.
2. Most of the fine structure emission in the EUV layer arises from 5–10 ($M_*/M_\odot$) AU. Most of the fine structure emission from the X-ray layer is distributed more broadly in r from $\lesssim$1 to 10 AU for a solar mass star.
3. If $L_X \sim L_{\rm EUV}$, there is about 2 times as much [Ne II] emission arising from the X-ray layer as from the EUV layer, assuming our standard "soft" EUV (30,000 K blackbody) spectrum that produces the most [Ne II] luminosity.
4. A power-law EUV spectrum, $L_\nu \propto \nu^{-1}$, results in a [Ne III] line luminosity that is greater than the [Ne II] line luminosity from the EUV layer, in contrast to observations. If the EUV layer is responsible for the [Ne II] emission, the EUV spectrum must be softer than an ~30,000–40,000 K blackbody spectrum between 15 eV and 40 eV. The X-ray layer, which has much higher abundances of atomic hydrogen, naturally gives [Ne III] line luminosities that are less than 0.1 of the [Ne II] luminosities because of rapid charge exchange reactions of Ne^{++} with H.
5. Internal shocks in protostellar winds may be a viable explanation of the observed [Ne II] in a number of sources, especially those with high $\dot{M}_{\rm w}$ or its surrogate $\dot{M}_{\rm acc}$. Confirmation of this origin requires high spatial ($\lesssim$1″) and spectral ($\lesssim$10 km s^{-1}) observations. The [Ne II] from these regions, if they are nearby, may be extended ($\gtrsim$1″) and should produce broader (~100 km s^{-1} FWHM) profiles than the [Ne II] from the EUV or X-ray layer, especially in face-on disks.
6. O I 6300 Å is weak ($L_{\rm [O\,I]} \lesssim 10^{-6}$) from the EUV layer, the transition layer between the EUV layer and the X-ray layer, the X-ray layer if the spectrum is dominated by 1–2 keV photons, and likely also the shear layer where the protostellar wind impacts the disk surface. A soft X-ray spectrum ($L_\nu \propto \nu^{-1}$ for 0.1 keV < $h\nu$ < 2 keV) with considerable luminosity in 0.1–0.3 keV photons produces a hotter and more ionized X-ray layer, and substantially more [O I] 6300 Å luminosity because of the extreme temperature

sensitivity of this line. L_X as high as $10^{-2}\,L_\odot$ with this spectrum results in $L_{[\mathrm{O\,I}]} \sim 10^{-4}\,L_\odot$. The observed values of the LVC of [O I] range from 10^{-6} to $10^{-3}\,L_\odot$, with typical values $\sim 10^{-4}\,L_\odot$. Therefore, soft X-rays are a plausible origin for the low velocity [O I] component in many sources.

7. We compared our models with a compilation of 54 sources of [Ne II] emission from young low-mass protostellar sources and with correlations of $L_{[\mathrm{Ne\,II}]}$ with L_X and $\dot{M}_{\mathrm{acc}}$. We note in point 5 that internal shocks in winds may be a viable explanation for especially the sources with observed outflows or jets. There are also sources with low $\dot{M}_{\mathrm{acc}}$ where our "harder" X-ray spectrum, with most luminosity emerging at 1–2 keV, can explain the observed [Ne II] emission. In some cases, the lines are resolved to be relatively narrow (10–60 km s^{-1}), further indicating an X-ray layer origin and not a shock origin. However, there exist sources where neither wind shocks nor 1–2 keV X-rays carry sufficient energy to power the observed [Ne II] line. These sources are likely candidates for [Ne II] originating from the EUV layer or from an excess of soft (∼0.1–0.3 keV) X-rays. If the spectrum in the EUV-soft X-ray wavelength region is a power law $L_\nu \propto \nu^{-1}$, as Ercolano et al. (2009) suggested, then the soft X-ray layer will dominate the production of [Ne II], although the EUV layer may produce more [Ne III] than the X-ray layer. Whichever layer dominates, the [Ne II] and [Ne III] luminosities directly provide a measure of the heretofore unobserved EUV or soft X-ray luminosities from the protostar or its immediate environs.

We thank R. Alexander, C. Clarke, J. Drake, B. Ercolano, A. Glassgold, M. Güdel, M. Kaufman, R. Meijerink, J. Najita, D. Neufeld, and I. Pascucci for helpful discussions and allowing us access to prepublication drafts of papers. We also thank R. Alexander for his helpful and thorough referee report and E. Feigelson, the editor, for helpful comments on the X-ray flare size, time variability, and spectral shape. We acknowledge financial support from NASA's Origins Program, Astrobiology Program, and Astrophysical Theory Program.

REFERENCES

Aldrovandi, S. M. V., & Pequignot, D. 1973, A&A, 25, 137
Alexander, R. D. 2008a, New Astron. Rev., 52, 60
Alexander, R. D. 2008b, MNRAS, 391, L64
Alexander, R. D., Clarke, C. J., & Pringle, J. E. 2004a, MNRAS, 354, 71
Alexander, R. D., Clarke, C. J., & Pringle, J. E. 2004b, MNRAS, 348, 879
Alexander, R. D., Clarke, C. J., & Pringle, J. E. 2005, MNRAS, 358, 283
Alexander, R. D., Clarke, C. J., & Pringle, J. E. 2006a, MNRAS, 369, 216
Alexander, R. D., Clarke, C. J., & Pringle, J. E. 2006b, MNRAS, 369, 229
Arnaud, M., & Rothenflug, R. 1985, A&AS, 60, 425
Asplund, M., Grevesse, N., & Sauval, A. J. 2005, in ASP Conf. Ser. 336, Cosmic Abundances as Records of Stellar Evolution and Nucleosynthesis, ed. T. G. Barnes & F. N. Bash (San Francisco, CA: ASP), 25
Balbus, S. A., & Hawley, J. F. 1991, ApJ, 376, 214
Blum, R. D., & Pradhan, A. K. 1992, ApJS, 80, 425
Brooks, D. H., Costa, V. M., Lago, M. T. V. T., & Lanzafame, A. C. 2001, MNRAS, 327, 177
Butler, K., & Zeippen, C. J. 1994, A&AS, 108, 1
Butler, S. E., & Dalgarno, A. 1980, ApJ, 241, 838
Chiang, E., & Murray-Clay, R. 2007, Nature Phys., 3, 604
Cieza, L. A., Swift, J. J., Mathews, G. S., & Williams, J. P. 2008, ApJ, 686, L115
Clarke, C. J., Gendrin, A., & Sotomayor, M. 2001, MNRAS, 328, 485
Dullemond, C. P., & Dominik, C. 2005, A&A, 434, 971
Ercolano, B., Clarke, C. C., & Drake, J. J. 2009, ApJ, 699, 1639
Ercolano, B., Drake, J. J., Raymond, J. C., & Clarke, C. C. 2008, ApJ, 688, 398
Espaillat, C., et al. 2007, ApJ, 664, L111
Favata, F., Flaccomio, E., Reale, F., Micela, G., Sciortino, S., Shang, H., Stassun, K. G., & Feigelson, E. D. 2005, ApJS, 160, 469
Favata, F., Micela, G., & Reale, F. 2001, A&A, 375, 485
Feigelson, E. D., & Montmerle, T. 1999, ARA&A, 37, 363
Flaccomio, E., Damiani, F., Micela, G., Sciortino, S., Harnden, F. R., Jr., Murray, S. S., & Wolk, S. J. 2003, ApJ, 582, 382
Font, A. S., McCarthy, I. G., Johnstone, D., & Ballantyne, D. R. 2004, ApJ, 607, 890
Franciosini, E., et al. 2007, A&A, 468, 485
Galavis, M. E., Mendoza, C., & Zeippen, C. J. 1995, A&AS, 111, 347
Getman, K. V., Feigelson, E. D., Broos, P. S., Micela, G., & Garmire, G. P. 2008a, ApJ, 688, 418
Getman, K. V., Feigelson, E. D., Micela, G., Jardine, M. M., Gregory, S. G., & Garmire, G. P. 2008b, ApJ, 688, 437
Glasse, A. C., Atad-Ettedgui, E. I., & Harris, J. W. 1997, Proc. SPIE, 2871, 1197
Glassgold, A. E., Ercolano, B., & Drake, J. J. 2009, ApJ, submitted
Glassgold, A. E., Najita, J., & Igea, J. 2004, ApJ, 615, 972
Glassgold, A. E., Najita, J. R., & Igea, J. 2007, ApJ, 656, 515
Gorti, U., Dullemond, C., & Hollenbach, D. 2009, ApJ, submitted
Gorti, U., & Hollenbach, D. 2004, ApJ, 613, 424
Gorti, U., & Hollenbach, D. 2008, ApJ, 683, 287
Gorti, U., & Hollenbach, D. 2009, ApJ, 690, 1539
Grevesse, N., & Sauval, A. J. 1998, Space Sci. Rev., 85, 161
Griffin, D. C., Mitnik, D. M., & Badnell, N. R. 2001, J. Phys. B: At. Mol. Phys., 34, 4401
Grosso, N., Montmerle, T., Feigelson, E. D., & Forbes, T. G. 2004, A&A, 419, 653
Güdel, M., Skinner, S. L., Audard, M., Briggs, K. R., & Cabrit, S. 2008, A&A, 478, 797
Güdel, M., Skinner, S. L., Mel'Nikov, S. Y., Audard, M., Telleschi, A., & Briggs, K. R. 2007, A&A, 468, 529
Güdel, M., & Telleschi, A. 2007, A&A, 474, L25
Güdel, M., et al. 2009, in New Light on Young Stars: Spitzer's View of Circumstellar Disks (Pasadena, CA: CalTech), http://www.ipac.caltech.edu/spitzer2008/talks/ManuelGuedel.html
Gullbring, E., Hartmann, L., Briceno, C., & Calvet, N. 1998, ApJ, 492, 323
Hartigan, P., Edwards, S., & Ghandour, L. 1995, ApJ, 452, 736
Hartmann, L., Calvet, N., Gullbring, E., & D'Alessio, P. 1998, ApJ, 495, 385
Herczeg, G. J., Najita, J. R., Hillenbrand, L. A., & Pascucci, I. 2007, ApJ, 670, 509
Ho, L. C., & Keto, E. 2007, ApJ, 658, 314
Hollenbach, D., Johnstone, D., Lizano, S., & Shu, F. 1994, ApJ, 428, 654
Hollenbach, D., & McKee, C. F. 1989, ApJ, 342, 306 (HM89)
Hollenbach, D. J., Yorke, H. W., & Johnstone, D. 2000, in Protostars and Planets IV, ed. V. Mannings, A. P. Boss, & S. S. Russell (Tucson, AZ: Univ. Arizona Press), 401
Kastner, J. H., Huenemoerder, D. P., Schulz, N. S., Canizares, C. R., & Weintraub, D. A. 2002, ApJ, 567, 434
Kingdon, J. B., & Ferland, G. J. 1996, ApJS, 106, 205
Lacy, J. H., Richter, M. J., Greathouse, T. K., Jaffe, D. T., & Zhu, Q. 2002, PASP, 114, 153
Lagage, P. O., et al. 2004, Messenger, 117, 12
Lahuis, F., van Dishoeck, E. F., Blake, G. A., Evans, N. J., II, Kessler-Silacci, J. E., & Pontoppidan, K. M. 2007, ApJ, 665, 492
Lecar, M., & Sasselov, D. D. 2003, ApJ, 596, L99
Lennon, D. J., & Burke, V. M. 1994, A&AS, 103, 273
Maloney, P. R., Hollenbach, D. J., & Tielens, A. G. G. M. 1996, ApJ, 466, 561
Matsuyama, I., Johnstone, D., & Hartmann, L. 2003, ApJ, 582, 893
Matsuyama, I., Johnstone, D., & Hollenbach, D. 2009, ApJ, 700, 10 (MJH09)
Meijerink, R., Glassgold, A. E., & Najita, J. R. 2008, ApJ, 676, 518
Muzerolle, J., Calvet, N., Briceño, C., Hartmann, L., & Hillenbrand, L. 2000, ApJ, 535, L47
Najita, J. R., Carr, J. S., Glassgold, A. E., & Valenti, J. A. 2007, in Protostars and Planets V, ed. B. Reipurth, D. Jewitt, & K. Keil (Tucson, AZ: Univ. Arizona Press), 507
Najita, J. R., et al. 2009, ApJ, 697, 957
Ouyed, R., & Pudritz, R. E. 1997, ApJ, 482, 712
Pascucci, I., & Sterzik, M. 2009, ApJ, in press
Pascucci, I., et al. 2007, ApJ, 663, 383
Pelan, J., & Berrington, K. A. 1995, A&AS, 110, 209
Preibisch, T. 2007, Mem. Soc. Astron. Ital., 78, 332
Ratzka, T., Leinert, C., Henning, T., Bouwman, J., Dullemond, C. P., & Jaffe, W. 2007, A&A, 471, 173
Ribas, I., Guinan, E. F., Güdel, M., & Audard, M. 2005, ApJ, 622, 680
Richling, S., Hollenbach, D., & Yorke, H. W. 2006, in Planet Formation, ed. H. Klahr & W. Brandner (Cambridge: Cambridge Univ. Press), 31

Ruden, S. P. 2004, ApJ, 605, 880
Safier, P. N. 1993a, ApJ, 408, 115
Safier, P. N. 1993b, ApJ, 408, 148
Salyk, C., Blake, G. A., Boogert, A. C. A., & Brown, J. M. 2009, ApJ, 699, 330
Sano, T., Miyama, S. M., Umebayashi, T., & Nakano, T. 2000, ApJ, 543, 486
Savage, B. D., & Sembach, K. R. 1996, ARA&A, 34, 279
Schmitt, J. H. M. M., & Robrade, J. 2007, A&A, 462, L41
Schneider, P. C., & Schmitt, J. H. M. M. 2008, A&A, 488, L13
Shu, F. H., Johnstone, D., & Hollenbach, D. 1993, Icarus, 106, 92
Shu, F., Najita, J., Ostriker, E., Wilkin, F., Ruden, S., & Lizano, S. 1994, ApJ, 429, 781
Shull, J. M., & van Steenberg, M. 1982, ApJS, 48, 95
Stelzer, B., Flaccomio, E., Briggs, K., Micela, G., Scelsi, L., Audard, M., Pillitteri, I., & Güdel, M. 2007, A&A, 468, 463
Stelzer, B., & Schmitt, J. H. M. M. 2004, A&A, 418, 687
Stone, J. M., & Pringle, J. E. 2001, MNRAS, 322, 461
Storey, P. J., & Hummer, D. G. 1995, MNRAS, 272, 41
Strom, S. E., Edwards, S., & Skrutskie, M. F. 1990, in ASP Conf. Ser. 9, Cool Stars, Stellar Systems, and the Sun, ed. G. Wallerstein (San Francisco, CA: ASP), 275
Tayal, S. S. 2000, ApJ, 530, 1091
Tayal, S. S., & Gupta, G. P. 1999, ApJ, 526, 544
Valenti, J. A., Fallon, A. A., & Johns-Krull, C. M. 2003, ApJS, 147, 305
van Boekel, R., Güdel, M., Henning, T., Lahuis, F., & Pantin, E. 2009, A&A, 497, 137
Veras, D., & Armitage, P. J. 2004, MNRAS, 347, 613
Verner, D. A., Ferland, G. J., Korista, K. T., & Yakovlev, D. G. 1996, ApJ, 465, 487
White, R. J., & Hillenbrand, L. A. 2004, ApJ, 616, 998
Wilms, J., Allen, A., & McCray, R. 2000, ApJ, 542, 914